

Secular precessing compact binary dynamics, spin and orbital angular momentum flip-flops

Márton Tápai[†], Zoltán Keresztes[‡], László Árpád Gergely^{*}

Institute of Physics, University of Szeged, Dóm tér 9, Szeged 6720, Hungary

[†]*E-mail: tapai@titan.physx.u-szeged.hu* [‡]*E-mail: zkeresztes@titan.physx.u-szeged.hu* ^{*}*E-mail: gergely@physx.u-szeged.hu*

We derive the conservative secular evolution of precessing compact binaries to second post-Newtonian order accuracy, with leading-order spin-orbit, spin-spin and mass quadrupole-monopole contributions included. The emerging closed system of first-order differential equations evolves the pairs of polar and azimuthal angles of the spin and orbital angular momentum vectors together with the periastron angle. In contrast with the instantaneous dynamics, the secular dynamics is autonomous. This secular dynamics reliably characterizes the system over timescales starting from a few times the radial period to several precessional periods, but less than the radiation reaction timescale. We numerically compare the instantaneous and secular evolutions and estimate the number of periods for which dissipation has no significant effect, e.g. the conservative timescale. We apply the analytic equations to study the spin flip-flop effect, recently found by numerical relativity methods. Our investigations show that the effect does not generalize beyond its original parameter settings, although we reveal distinct configurations exhibiting one half flip-flops. In addition, we find a flip-flopping evolution of the orbital angular momentum vector, which ventures from one pole to another through several precessional periods. This is a new effect, occurring for mass ratios much less than one.

PACS numbers:

I. INTRODUCTION

The LIGO collaboration with the improved Advanced LIGO detectors [1], has recently announced its first two detections of gravitational waves from coalescing stellar mass black hole binaries [2],[3]. With the approaching second observation run, the era of gravitational wave astrophysics has commenced.

Whenever the black hole spins \mathbf{S}_1 , \mathbf{S}_2 and the orbital angular momentum \mathbf{L}_N of the binary do not align, they undergo precession. The total angular momentum $\mathbf{J} = \mathbf{L}_N + \mathbf{S}_1 + \mathbf{S}_2$ is conserved up to the 2 post-Newtonian (PN) order. The gravitational waveform emitted by the system exhibits both amplitude and phase modulations due to precession. Detection of precessing gravitational waves requires corresponding waveforms, such as the analytic frequency domain waveform developed in Ref. [4]. The consequences of precession on gravitational waveforms were presented in Refs. [5]-[10]. In Refs. [11]-[40] the precessing conventions and various spin related contributions were discussed, while Refs. [41]-[43] analysed the searches for spin-precessing binaries. The 4PN spin dependent conservative dynamics of inspiralling compact binaries was completed in Ref. [44]. A fully precessing analysis of the first gravitational wave detection GW150914 was presented in Ref. [45].

Compact binary dynamics in the inspiral regime exhibit three distinct timescales. The shortest is the radial timescale, defined by the radial period. The precessional timescale is given by the time necessary for the orbital angular momentum \mathbf{L}_N or for the spins \mathbf{S}_1 , \mathbf{S}_2 to undergo a full rotation about their precession axis. The third is the gravitational radiation reaction timescale, over which the effects of gravitational dissipation are noticeable.

Averaging the dynamics over some of these timescales may turn useful. When precession related effects are examined, averaging over a radial period will remove insignificant instantaneous effects, but keeps the precessional evolution, which will be dominant. Precession related effects like the spin-flip [46], explaining the formation of X-shape radio galaxies [47], and transitional precession [48] were examined with this method. Precession of the dominant spin of a supermassive black hole binary was also identified for the first time from VLBI radio data of its jet spanning over 18 years in Ref. [49]. For gravitational dissipation, averaging over the precessional period may turn useful.

The instantaneous dynamics (including spin effects) in terms of dimensionless variables was discussed in Refs. [50] - [52]. This generalizes earlier works on binary dynamics of Refs. [53] - [58].

In this paper we investigate compact binary systems which are subject to bound motion, establishing the 2PN secular dynamics. In Section II we will derive the radial period in terms of the averaged values of the dimensionless orbital angular momentum

$$\mathfrak{l}_r = \frac{cL_N}{Gm\mu}, \quad (1)$$

and dimensionless eccentricity

$$e_r = \frac{A_N}{Gm\mu}. \quad (2)$$

These two parameters characterize the shape of the orbit in the plane of the motion. Hence they will be dubbed shape variables. The total mass of the binary is $m = m_1 + m_2$, $\mu = m_1 m_2 / m$ is the reduced mass, G is the gravitational constant, c is the speed of light and A_N is

the magnitude of the Laplace-Runge-Lenz vector. Other notations frequently used in this paper are the mass ratio $\nu = m_2/m_1$ and the symmetric mass ratio $\eta = \mu/m$. The magnitude of the spins is given by the dimensionless spin parameters χ_i ($i = 1, 2$). A dimensionless time variable $\mathfrak{t} = tc^3/Gm$ (with time t) was introduced in Ref. [52]. Derivatives with regards to the dimensionless time are denoted by a dot.

Auxiliary calculations required for the radial period will be given in Appendices A-C. Appendix A presents the radial period in terms of the variables evaluated at the periastron (characterized by the value of the true anomaly parameter $\chi_p = 0$). The χ_p dependence of the shape variables is also derived in this Appendix. Appendix B contains the averaged shape variables. In Appendix C we express the shape variables evaluated in the periastron with the corresponding averaged quantities.

In Section III we present the main result of the paper, which is the *secular* precessing compact binary dynamics. For completeness, in Appendix D we give the secular precession angular velocities. In Section IV we investigate the limits of validity of the secular dynamics, establishing the corresponding conservative timescale.

When the dominant spin vector approximately lies in the plane of motion, while the smaller spin is closely aligned with the orbital angular momentum \mathbf{L}_N , the smaller spin slowly evolves to be anti aligned with \mathbf{L}_N , then periodically changes back and forth on a timescale shorter than the gravitational radiation reaction timescale. This effect, dubbed flip-flop has been established by numerical relativity methods in Refs. [59] - [61]. In Section V we examine the parameter dependence of the spin flip-flop phenomenon, as an application of the derived secular dynamics. We reproduce analytically the flip-flop effect in its original parameter settings, then we find parameter ranges where only a half flip-flop occurs, but for both spins.

In Section VI we discuss a parameter configuration for which the orbital angular momentum undergoes a similar flip-flopping, a behaviour unaccounted before.

In Section VII we give the conclusions.

II. INTEGRATION OF THE INSTANTANEOUS DYNAMICS

The 2PN conservative dynamics of compact binary systems was given as Eqs. (36)-(42) of Ref. [52] in terms of dimensionless osculating orbital elements \mathfrak{l}_r , e_r , ψ_p , α , ϕ_n , spin polar and azimuthal angles κ_i and ζ_i ($i = 1, 2$), the true anomaly parametrization χ_p . The time evolution of χ_p is governed by Eq. (43) of Ref. [52]. The polar and azimuthal angles of the spins are defined in a system with \mathbf{L}_N as the z-axis and \mathbf{A}_N as the x-axis. The argument of the periastron, ψ_p is defined by $\psi_p = \arccos(\hat{\mathbf{l}} \cdot \hat{\mathbf{A}}_N)$, with $\hat{\mathbf{l}} = \hat{\mathbf{J}} \times \hat{\mathbf{L}}_N$. The inclination α is the polar angle of $\hat{\mathbf{L}}_N$ in the system where the z-axis points in the direction

of $\hat{\mathbf{J}}$, and the x-axis is given by $\hat{\mathbf{l}}$. The last angle is the longitude of the ascending node $-\phi_n$, span by the inertial axis $\hat{\mathbf{x}}$ (arbitrarily chosen in the plane perpendicular to $\hat{\mathbf{J}}$) and $\hat{\mathbf{l}}$. This angle becomes the azimuthal angle of $\hat{\mathbf{L}}_N$, if initially $\hat{\mathbf{L}}_N$ is set in the plane defined by $\hat{\mathbf{x}}$ and $\hat{\mathbf{J}}$.

The main purpose of this paper is to average this instantaneous dynamics over a radial period, to 2PN order. For bounded motion, by definition the dimensionless period $\mathfrak{T} \equiv Tc^3/Gm$, referring to a change in the true anomaly $\chi_p \in \{0, 2\pi\}$, can be computed as

$$\mathfrak{T} \equiv \int_0^{\mathfrak{T}} dt = \int_0^{2\pi} \frac{1}{\dot{\chi}_p} d\chi_p. \quad (3)$$

By formally integrating (3) we get the following PN expansion:

$$\mathfrak{T} = \mathfrak{T}_0 \left(1 + \frac{\tau_{0PN}}{\mathfrak{l}_r^2} + \frac{\tau_{0SO}}{\mathfrak{l}_r^3} + \frac{\tau_{0SS}}{\mathfrak{l}_r^4} + \frac{\tau_{0QM}}{\mathfrak{l}_r^4} + \frac{\tau_{02PN}}{\mathfrak{l}_r^4} \right). \quad (4)$$

Here $1/\mathfrak{l}_r^2$ stands for one PN order, as explained in Ref. [52], while the lower index 0 indicates values taken at $\chi_p = 0$. In order to explicitly compute the terms of Eq. (4), the χ_p dependence of \mathfrak{l}_r and e_r are required. Their derivation and explicit expressions are given in Appendix A.

A different expansion of the period arises in terms of the averaged shape variables $\bar{\mathfrak{l}}_r$ and \bar{e}_r :

$$\mathfrak{T} = \tilde{\mathfrak{T}} \left(1 + \frac{1}{\bar{\mathfrak{l}}_r^2} \tilde{\tau}_{PN} + \frac{1}{\bar{\mathfrak{l}}_r^3} \tilde{\tau}_{SO} + \frac{1}{\bar{\mathfrak{l}}_r^4} \tilde{\tau}_{QM} + \frac{1}{\bar{\mathfrak{l}}_r^4} \tilde{\tau}_{SS} + \frac{1}{\bar{\mathfrak{l}}_r^4} \tilde{\tau}_{2PN} \right). \quad (5)$$

Here

$$\tilde{\mathfrak{T}} = \frac{2\bar{\mathfrak{l}}_r^3 \pi}{(1 - \bar{e}_r^2)^{3/2}}, \quad (6)$$

$$\tilde{\tau}_{PN} = \sqrt{1 - \bar{e}_r^2} (15 - 9\eta) + (1 - \bar{e}_r^2) (7\eta - 6), \quad (7)$$

$$\tilde{\tau}_{SO} = 0, \quad (8)$$

$$\tilde{\tau}_{2PN} = \frac{\sqrt{1 - \bar{e}_r^2}}{64\bar{e}_r^4} \sum_{k=0}^6 \bar{U}_k \bar{e}_r^k - \frac{(\bar{e}_r + 1)}{8\bar{e}_r^4} \sum_{k=0}^7 \bar{V}_k \bar{e}_r^k, \quad (9)$$

$$\tilde{\tau}_{QM} = \frac{3\eta}{512\bar{e}_r (1 - \bar{e}_r^2)^2 \bar{\mathfrak{l}}_r^2} \sum_{k=1}^2 \chi_k^2 \nu^{2k-3} w_k \times [\bar{U}^{QM} \sin^2 \kappa_k \cos 2\zeta_k + \bar{V}^{QM} (3 \cos 2\kappa_k + 1)], \quad (10)$$

$$\tilde{\tau}_{SS} = \frac{3\chi_1 \chi_2 \eta}{8(1 - \bar{e}_r)^2 \bar{e}_r} (\cos \kappa_1 \cos \kappa_2 \bar{U}^{SS} + \sin \kappa_1 \sin \kappa_2 \bar{V}^{SS}). \quad (11)$$

TABLE I: The coefficients in Eqs (9)-(11).

<i>Coefficient</i>	<i>Expression</i>
\bar{U}_6	$-437\eta^2 + 3336\eta - 1008$
\bar{U}_5	$-64(8\eta^2 - 6\eta - 5)$
\bar{U}_4	$-8(211\eta^2 - 159\eta + 336)$
\bar{U}_3	$64(4\eta^2 + 11\eta - 5)$
\bar{U}_2	$-8(79\eta^2 - 600\eta + 528)$
\bar{U}_1	$-128(\eta^2 - 8\eta + 15)$
\bar{U}_0	$32(65\eta^2 - 238\eta + 180)$
\bar{V}_7	$224\eta^2 - 690\eta + 360$
\bar{V}_6	$2(64\eta^2 - 11\eta - 12)$
\bar{V}_5	$139\eta^2 - 410\eta + 452$
\bar{V}_4	$-179\eta^2 + 266\eta - 308$
\bar{V}_3	$-27\eta^2 + 28\eta + 8$
\bar{V}_2	$67\eta^2 - 4\eta + 72$
\bar{V}_1	$-12(23\eta^2 - 90\eta + 80)$
\bar{V}_0	$260\eta^2 - 952\eta + 720$
\bar{U}^{QM}	$-4(27\bar{e}_r^7 - 72\bar{e}_r^6 + 263\bar{e}_r^5 - 1674\bar{e}_r^4 - 1702\bar{e}_r^3 - 4116\bar{e}_r^2 - 1360\bar{e}_r - 960)$
\bar{V}^{QM}	$16(\bar{e}_r^7 - 2\bar{e}_r^6 + 9\bar{e}_r^5 - 43\bar{e}_r^4 - 69\bar{e}_r^3 - 108\bar{e}_r^2 - 46\bar{e}_r - 12)$
\bar{U}^{SS}	$-8\bar{e}_r^5 + 21\bar{e}_r^4 - 15\bar{e}_r^3 - 38\bar{e}_r^2 - 56\bar{e}_r - 24$
\bar{V}^{SS}	$\frac{\cos(\zeta_1 - \zeta_2)}{2} (8\bar{e}_r^5 - 21\bar{e}_r^4 + 15\bar{e}_r^3 + 38\bar{e}_r^2 + 56\bar{e}_r + 24) + \frac{\cos(\zeta_1 + \zeta_2)}{4\bar{e}_r^2(\bar{e}_r + 1)} [371\bar{e}_r^7 - 276\bar{e}_r^6 + \bar{e}_r^5(-48\bar{e}_r + 104\sqrt{1 - \bar{e}_r^2} + 1771) - \bar{e}_r^4(48\bar{e}_r + 104\sqrt{1 - \bar{e}_r^2} + 1517) + 8\bar{e}_r^3(24\bar{e}_r + 583\sqrt{1 - \bar{e}_r^2} - 854) + 4\bar{e}_r^2(48\bar{e}_r - 1166\sqrt{1 - \bar{e}_r^2} + 1 + 1881) - 8(596\sqrt{1 - \bar{e}_r^2} - 593)\bar{e}_r + 4768(\sqrt{1 - \bar{e}_r^2} - 1)]$

The coefficients in the above expressions are enlisted in Table I.

The time average \bar{f} of any quantity $f(t)$ with respect to t has been defined as

$$\bar{f} = \int_0^{\mathfrak{T}} f(t) dt = \int_0^{2\pi} f(\chi_p) \frac{1}{\dot{\chi}_p} d\chi_p. \quad (12)$$

We note that for the change of variables from t to χ_p to be valid at a certain PN accuracy, \mathfrak{T} needs to be given at the same PN accuracy as $f(\chi_p)$.

Hence the average expressions of \bar{l}_r and \bar{e}_r are computed as

$$\bar{l}_r = \frac{1}{\mathfrak{T}} \int_0^{2\pi} \frac{l_r(\chi_p)}{\dot{\chi}_p} d\chi_p, \quad (13)$$

$$\bar{e}_r = \frac{1}{\mathfrak{T}} \int_0^{2\pi} \frac{e_r(\chi_p)}{\dot{\chi}_p} d\chi_p. \quad (14)$$

Integrating and Taylor-expanding to 2PN order accuracy leads to the following formal expressions

$$\bar{l}_r = \frac{l_{r0N} + \bar{l}_{rPN} + \bar{l}_{rSO} + \bar{l}_{rSS} + \bar{l}_{rQM} + \bar{l}_{r2PN}}{\mathfrak{T}}, \quad (15)$$

$$\bar{e}_r = \frac{e_{r0N} + \bar{e}_{rPN} + \bar{e}_{rSO} + \bar{e}_{rSS} + \bar{e}_{rQM} + \bar{e}_{r2PN}}{\mathfrak{T}}. \quad (16)$$

(The radial period is taken at 2PN accuracy.) The computation leading to the averaged shape variables is given in Appendix B, while the derivation of the shape variables at $\chi_p = 0$ in terms of the averaged quantities \bar{l}_r and \bar{e}_r in Appendix C.

III. SECULAR PRECESSING COMPACT BINARY DYNAMICS

In this section we give the main results of the paper, the averaged evolution equations of the dimensionless osculating orbital elements l_r , e_r , ψ_p , α , ϕ_n and spin angles κ_i , ζ_i ($i = 1, 2$). These equations contain post-Newtonian (PN), spin-orbit (SO), spin-spin (SS), quadrupole-monopole (QM) and second post-Newtonian (2PN) contributions.

A. Shape variables

The secular evolution equation of the dimensionless orbital angular momentum l_r reads as

$$\dot{\bar{l}}_r = \dot{\bar{l}}_r^{PN} = \dot{\bar{l}}_r^{SO} = \dot{\bar{l}}_r^{SS} = \dot{\bar{l}}_r^{QM} = \dot{\bar{l}}_r^{2PN} = 0. \quad (17)$$

The secular evolution equation of the dimensionless orbital eccentricity e_r also reads as

$$\dot{\bar{e}}_r = \dot{\bar{e}}_r^{PN} = \dot{\bar{e}}_r^{SO} = \dot{\bar{e}}_r^{SS} = \dot{\bar{e}}_r^{QM} = \dot{\bar{e}}_r^{2PN} = 0. \quad (18)$$

As expected, the average shape of the orbit does not change without dissipation.

B. Euler angles

The secular evolution equation of the three Euler angles are given below.

1. Inclination α

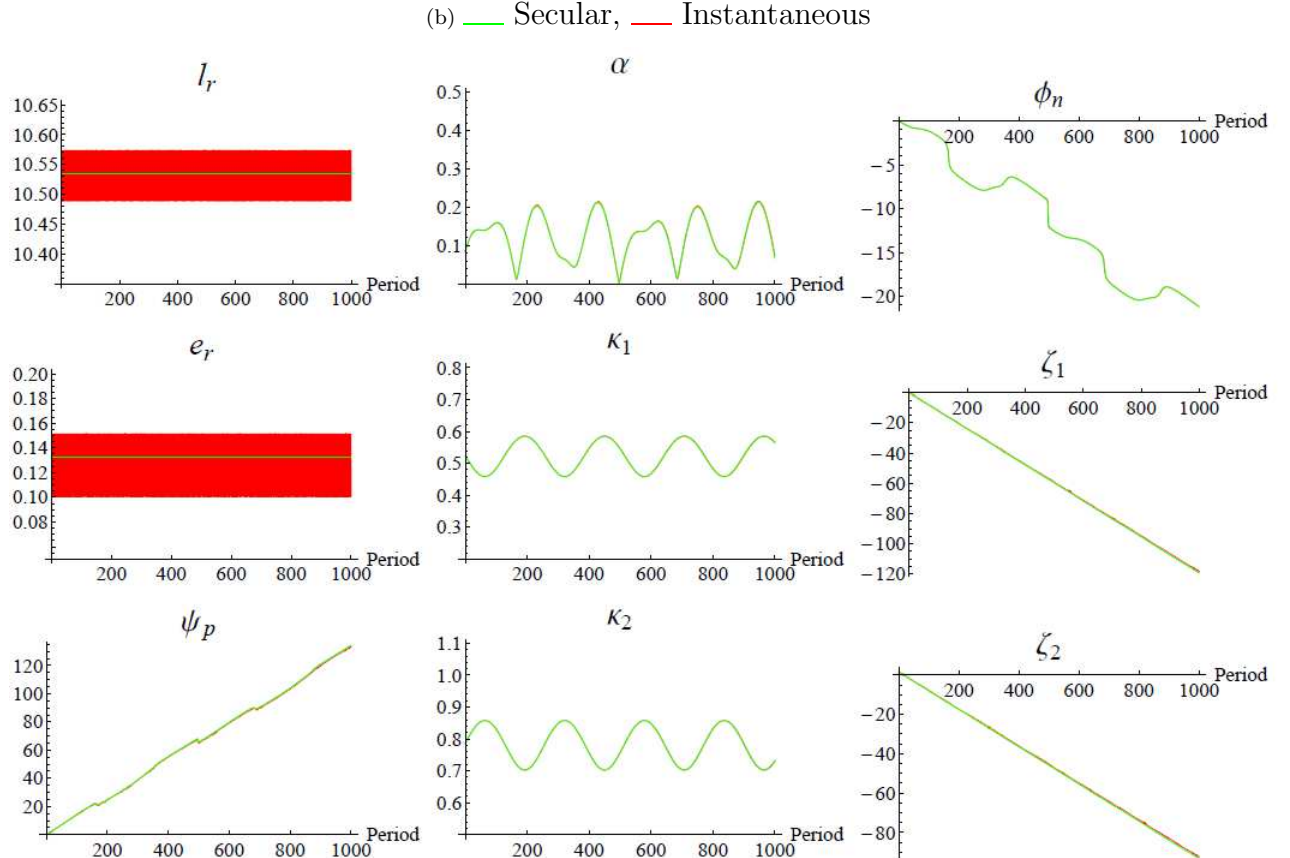
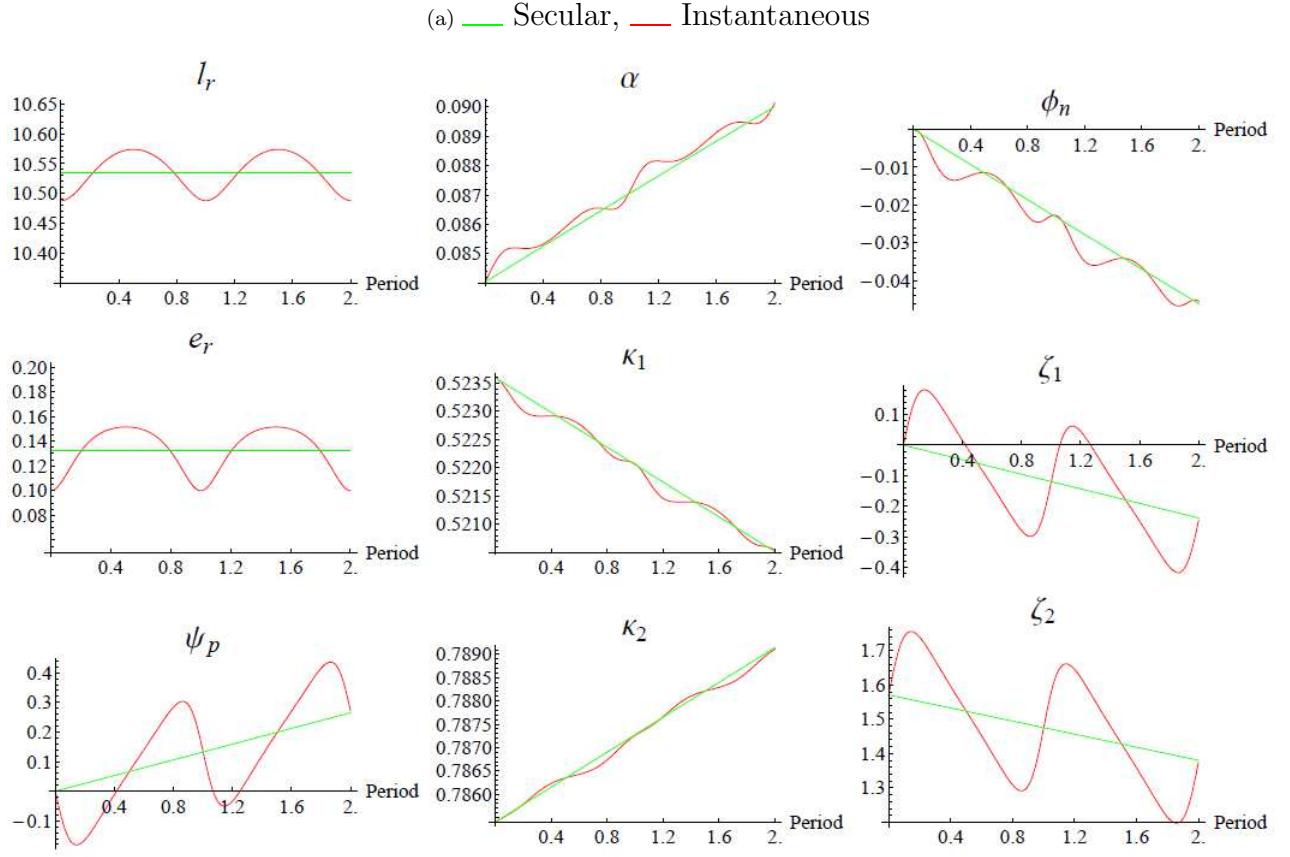


FIG. 1: Comparison of the secular and instantaneous dynamics. The upper block a) shows the first two periods, while the lower block b) is over the conservative timescale (shown as the corresponding number of periods on the x-axis). The figures are for total mass $m = 20M_\odot$, mass ratio $\nu = 0.5$, dimensionless spin parameters $\chi_1 = 0.9982$, $\chi_2 = 0.9982$, PN parameter $\varepsilon = 0.01$. The initial values of the other parameters are $e_r = 0.1$, $\kappa_1 = \pi/6$, $\kappa_2 = \pi/4$, $\zeta_1 = 0$, $\zeta_2 = \pi/2$, $\psi_p = 0$, $\phi_n = 0$.

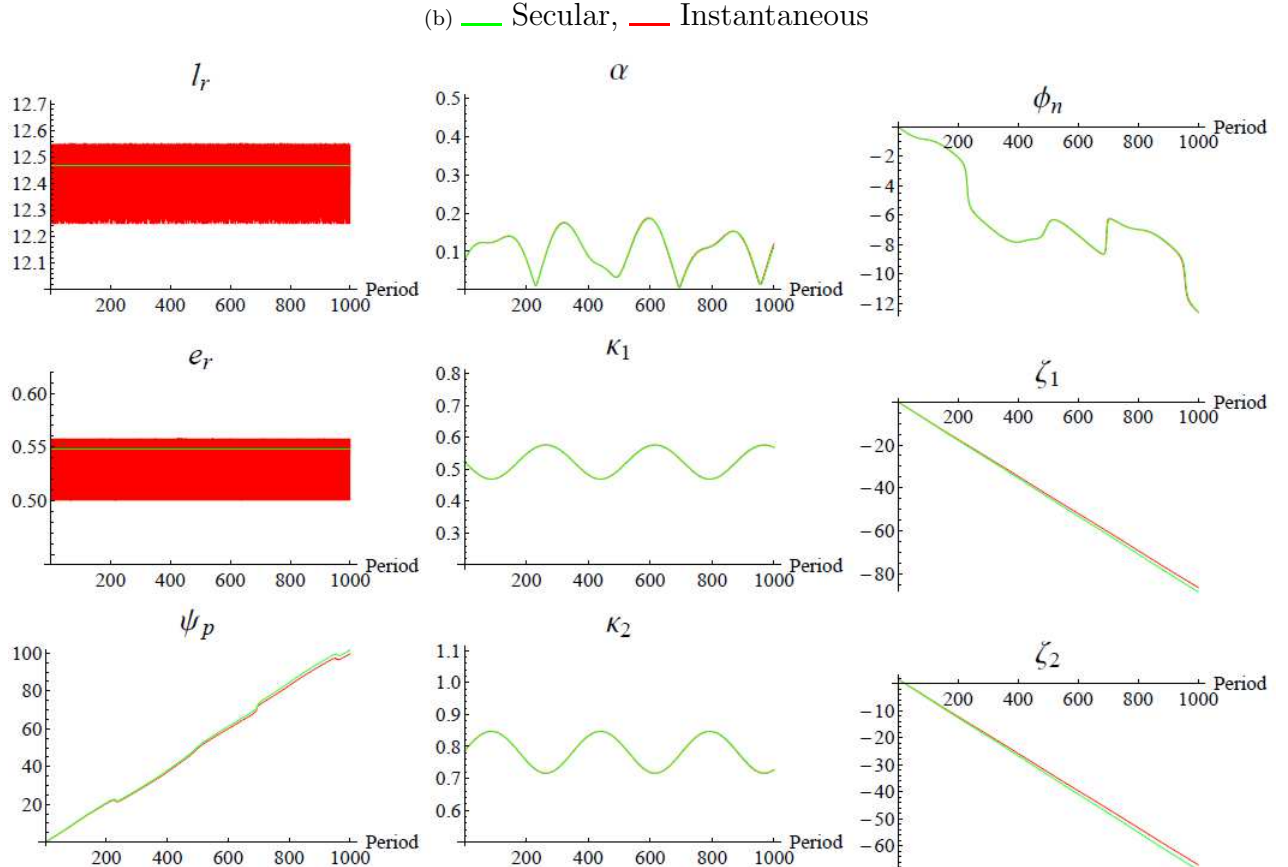
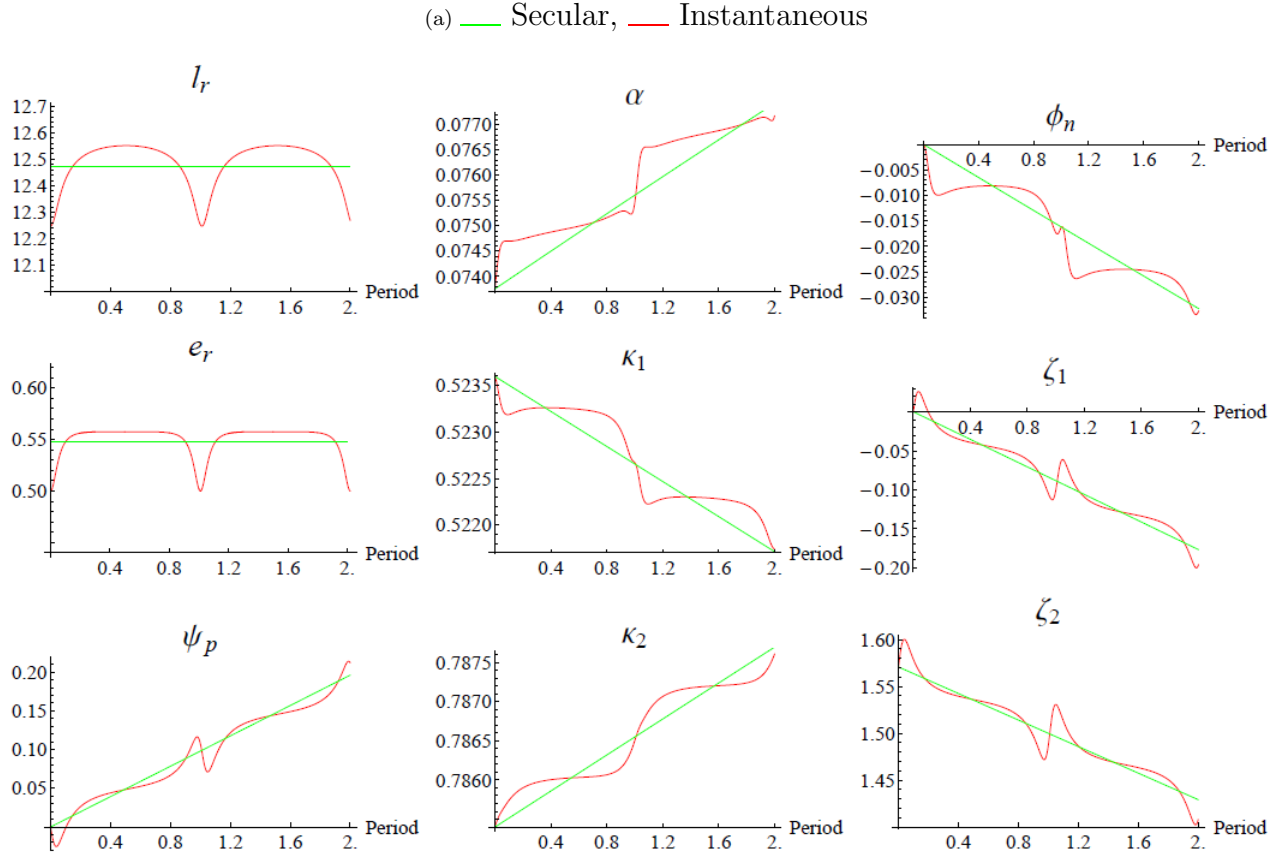


FIG. 2: Comparison of the secular and instantaneous dynamics. The upper block a) shows the first two periods, while the lower block b) is over the conservative timescale (shown as the corresponding number of periods on the x-axis). The figures are for total mass $m = 20M_{\odot}$, mass ratio $\nu = 0.5$, dimensionless spin parameters $\chi_1 = 0.9982$, $\chi_2 = 0.9982$, PN parameter $\varepsilon = 0.01$. The initial values of the other parameters are $e_r = 0.5$, $\kappa_1 = \pi/6$, $\kappa_2 = \pi/4$, $\zeta_1 = 0$, $\zeta_2 = \pi/2$, $\psi_p = 0$, $\phi_n = 0$.

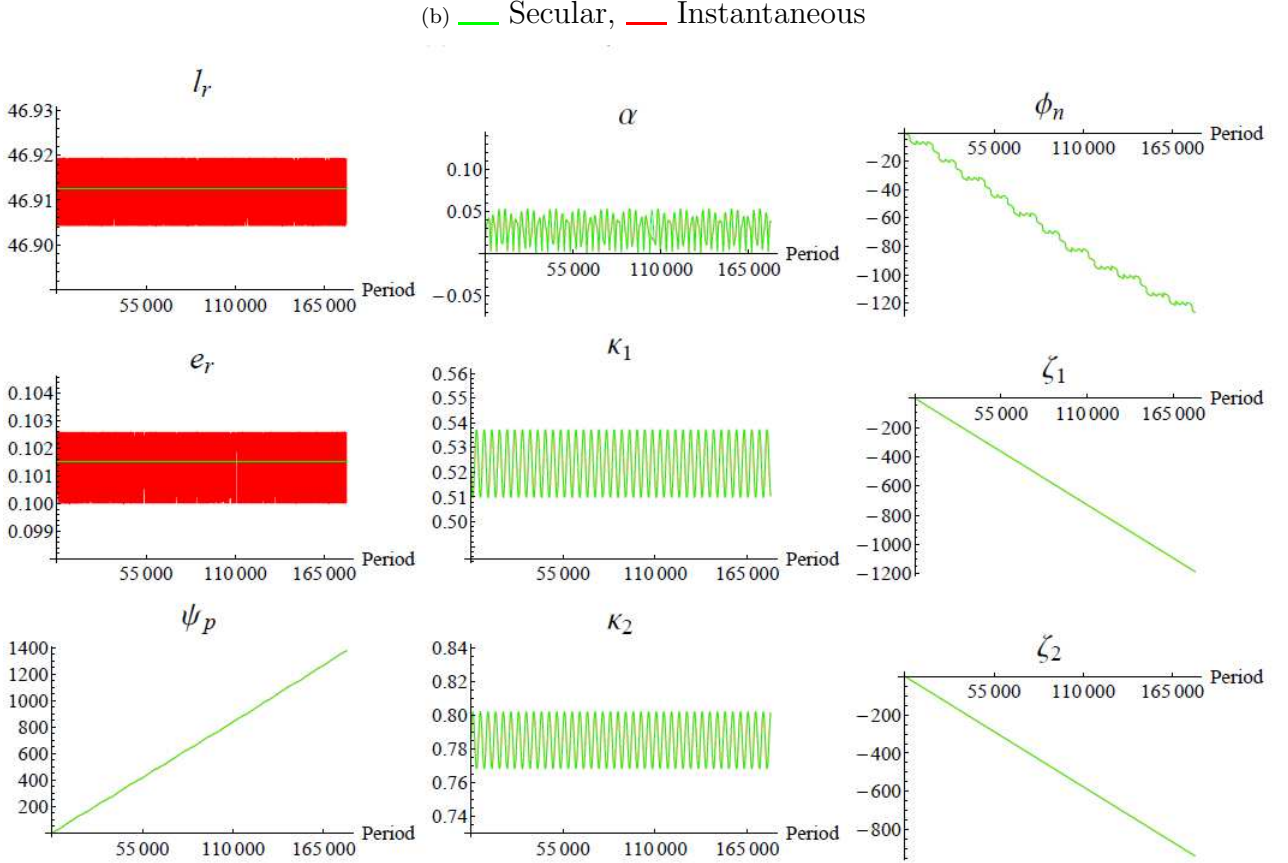
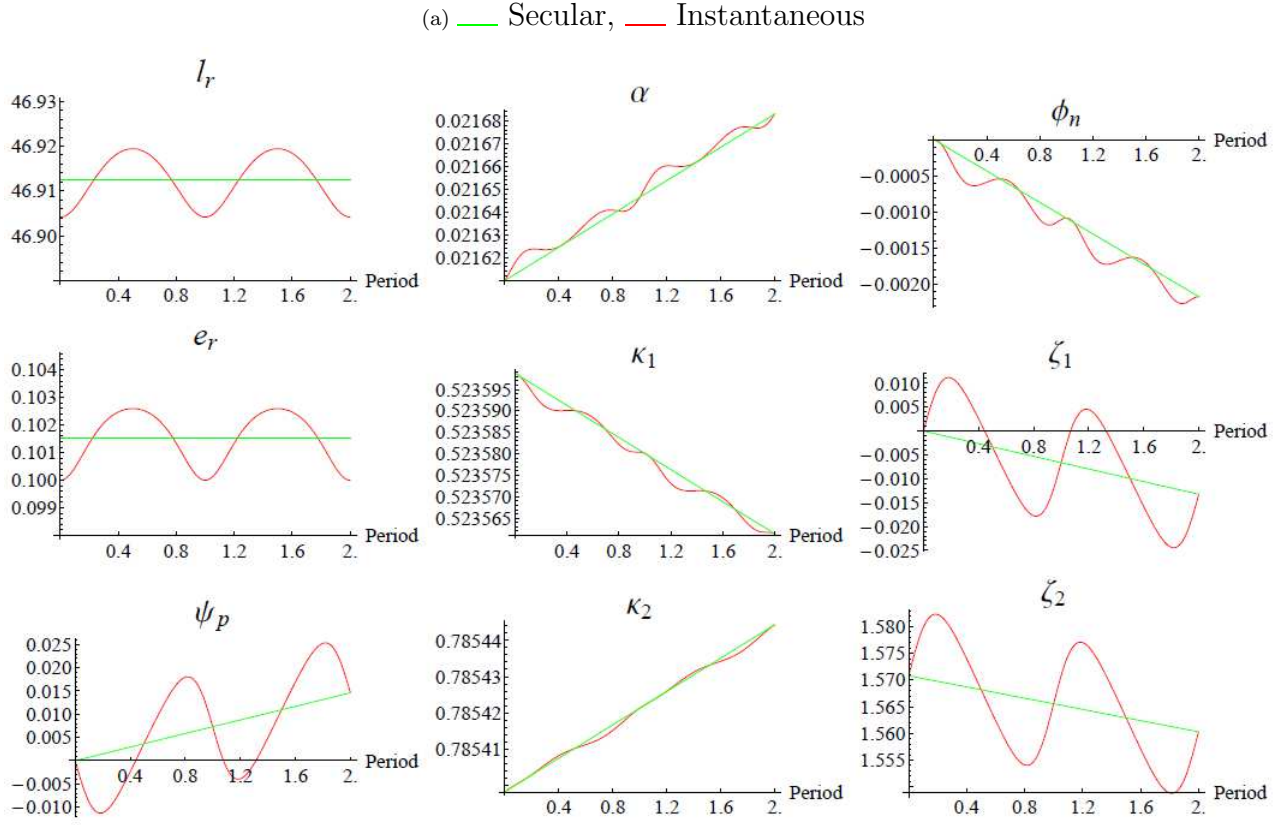


FIG. 3: Comparison of the secular and instantaneous dynamics. The upper block a) shows the first two periods, while the lower block b) is over the conservative timescale (shown as the corresponding number of periods on the x-axis, the conservative timescale being set as $N = 0.001\epsilon^{-5/2}$ number of periods). The figures are for total mass $m = 20M_\odot$, mass ratio $\nu = 0.5$, dimensionless spin parameters $\chi_1 = 0.9982$, $\chi_2 = 0.9982$, PN parameter $\epsilon = 0.0005$. The initial values of the other parameters are $e_r = 0.1$, $\kappa_1 = \pi/6$, $\kappa_2 = \pi/4$, $\zeta_1 = 0$, $\zeta_2 = \pi/2$, $\psi_p = 0$, $\phi_n = 0$.

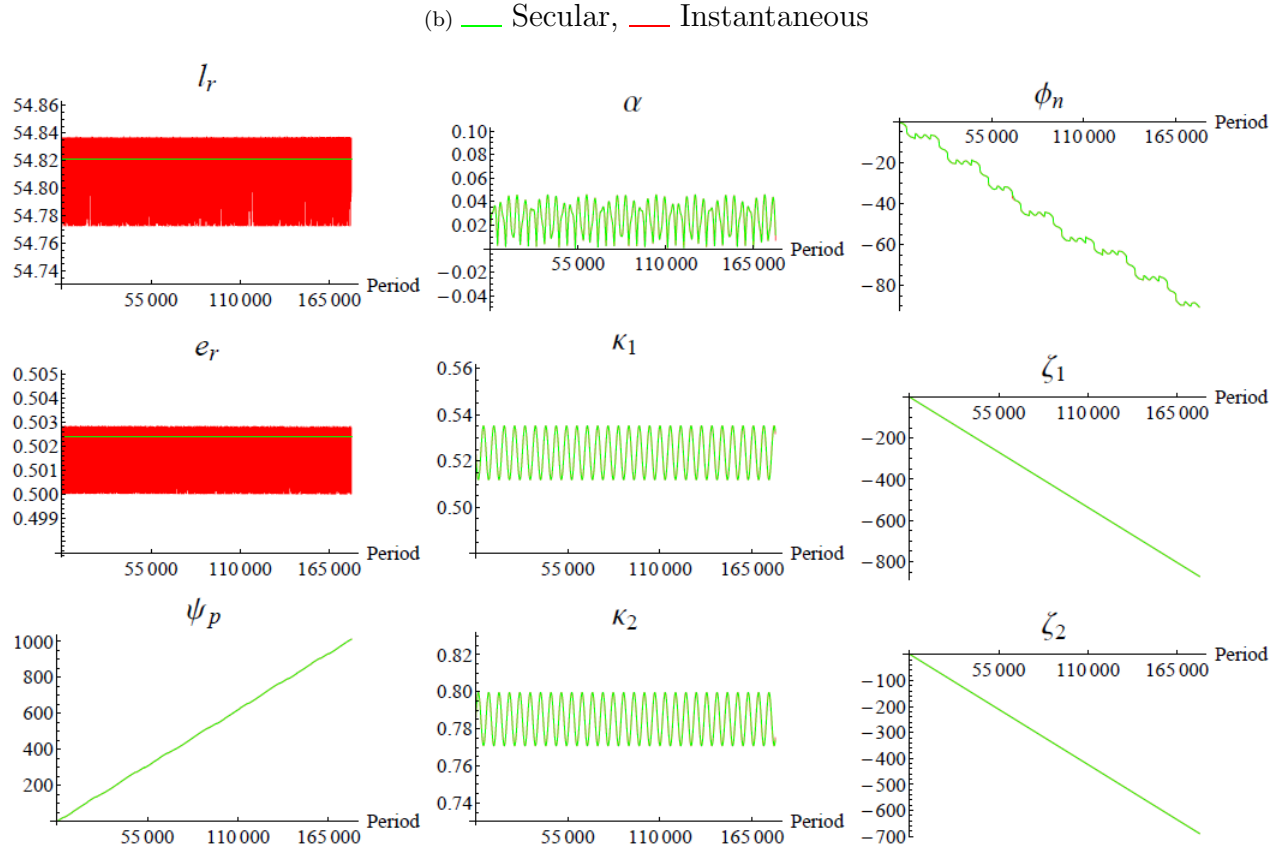
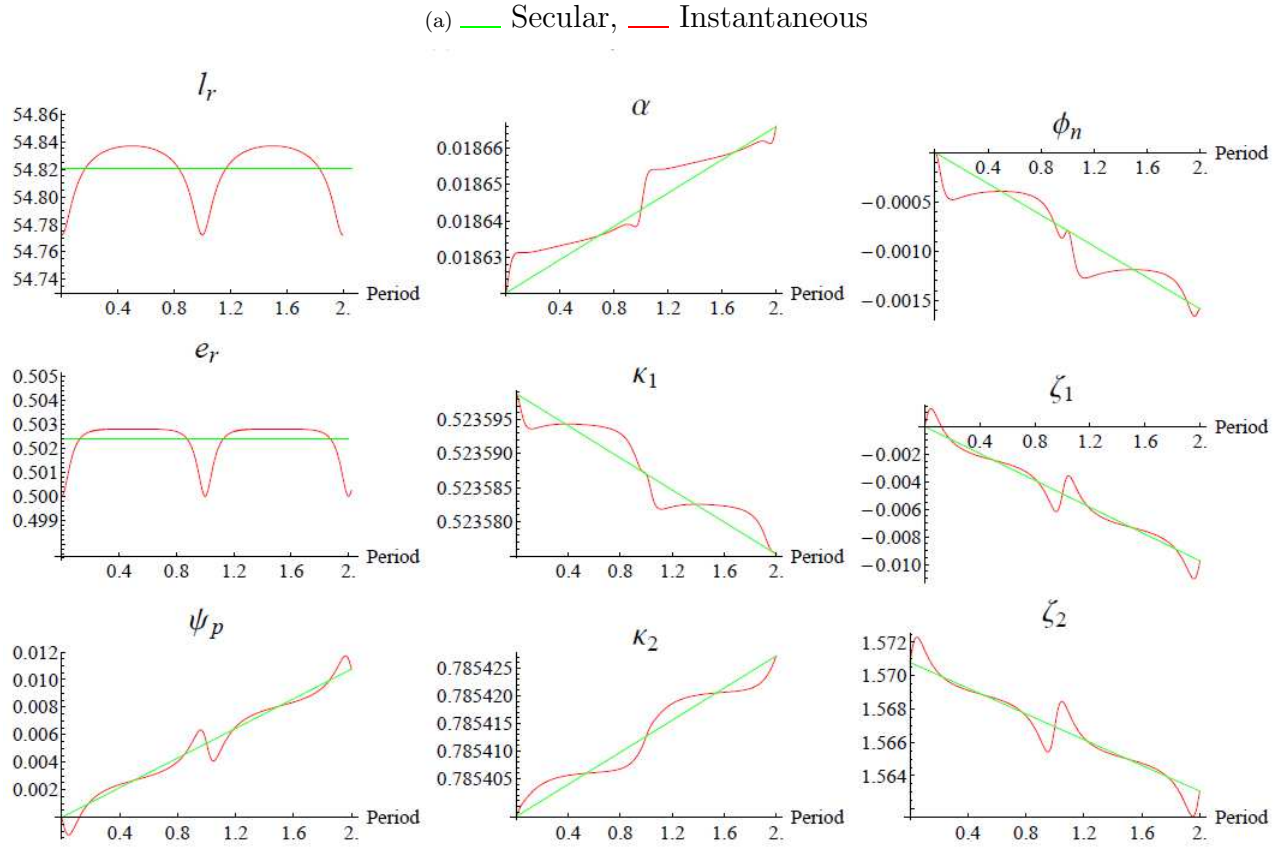


FIG. 4: Comparison of the secular and instantaneous dynamics. The upper block a) shows the first two periods, while the lower block b) is over the conservative timescale (shown as the corresponding number of periods on the x-axis, the conservative timescale being set as $N = 0.001\epsilon^{-5/2}$ number of periods). The figures are for total mass $m = 20M_\odot$, mass ratio $\nu = 0.5$, dimensionless spin parameters $\chi_1 = 0.9982$, $\chi_2 = 0.9982$, PN parameter $\epsilon = 0.0005$. The initial values of the other parameters are $e_r = 0.5$, $\kappa_1 = \pi/6$, $\kappa_2 = \pi/4$, $\zeta_1 = 0$, $\zeta_2 = \pi/2$, $\psi_p = 0$, $\phi_n = 0$.

The secular evolution of the inclination $\alpha = \arccos(\hat{\mathbf{J}} \cdot \hat{\mathbf{L}}_{\mathbf{N}})$ is given by the following contributions

$$\bar{\alpha}^{PN} = 0 , \quad (19)$$

$$\begin{aligned} \bar{\alpha}^{SO} &= \frac{\eta\pi}{\mathfrak{T} \bar{l}_r^3} \sum_{k=1}^2 (4\nu^{2k-3} + 3) \\ &\times \chi_k \sin \kappa_k \cos(\psi_p + \zeta_k) , \end{aligned} \quad (20)$$

$$\begin{aligned} \bar{\alpha}^{SS} &= -\frac{3\eta\pi}{\mathfrak{T} \bar{l}_r^4} \chi_1 \chi_2 \\ &\times [\sin \kappa_1 \cos \kappa_2 \cos(\psi_p + \zeta_1) \\ &+ \cos \kappa_1 \sin \kappa_2 \cos(\psi_p + \zeta_2)] , \end{aligned} \quad (21)$$

$$\begin{aligned} \bar{\alpha}^{QM} &= -\frac{3\eta\pi}{2\mathfrak{T} \bar{l}_r^4} \sum_{k=1}^2 \nu^{2k-3} w_k \chi_k^2 \\ &\times \sin 2\kappa_k \cos(\psi_p + \zeta_k) . \end{aligned} \quad (22)$$

$$\bar{\alpha}^{2PN} = 0 . \quad (23)$$

As expected, the inclination only changes due to spin and quadrupolar effects.

2. The longitude of the ascending node $-\phi_n$

The longitude of the ascending node $-\phi_n$ is subtended by the inertial axis $\hat{\mathbf{x}}$ and the ascending node $\hat{\mathbf{l}} = \hat{\mathbf{L}}_{\mathbf{N}} \times \hat{\mathbf{J}}$, it has the following contributions to its secular evolution

$$\bar{\phi}_n^{PN} = 0 , \quad (24)$$

$$\begin{aligned} \bar{\phi}_n^{SO} &= -\frac{\eta\pi}{\mathfrak{T} \bar{l}_r^3 \sin \alpha} \sum_{k=1}^2 (4\nu^{2k-3} + 3) \\ &\times \chi_k \sin \kappa_k \sin(\psi_p + \zeta_k) , \end{aligned} \quad (25)$$

$$\begin{aligned} \bar{\phi}_n^{SS} &= \frac{3\eta\pi}{\mathfrak{T} \bar{l}_r^4 \sin \alpha} \chi_1 \chi_2 \\ &\times [\sin \kappa_1 \cos \kappa_2 \sin(\psi_p + \zeta_1) \\ &+ \cos \kappa_1 \sin \kappa_2 \sin(\psi_p + \zeta_2)] , \end{aligned} \quad (26)$$

$$\begin{aligned} \bar{\phi}_n^{QM} &= \frac{3\eta\pi}{2\mathfrak{T} \bar{l}_r^4 \sin \alpha} \sum_{k=1}^2 \nu^{2k-3} w_k \chi_k^2 \\ &\times \sin 2\kappa_k \sin(\psi_p + \zeta_k) , \end{aligned} \quad (27)$$

$$\bar{\phi}_n^{2PN} = 0 . \quad (28)$$

Again, only spin and quadrupolar effects contribute.

3. Argument of the periastron ψ_p

The secular evolution of the angle ψ_p between the node line ($\hat{\mathbf{l}}$ perpendicular to both $\mathbf{L}_{\mathbf{N}}$ and \mathbf{J}) and the periastron ($\hat{\mathbf{A}}_{\mathbf{N}}$) is given by

$$\bar{\psi}_p^{PN} = \frac{6\pi}{\mathfrak{T} \bar{l}_r^2} , \quad (29)$$

$$\begin{aligned} \bar{\psi}_p^{SO} &= -\frac{\eta\pi}{\mathfrak{T} \bar{l}_r^3} \sum_{k=1}^2 (4\nu^{2k-3} + 3) \\ &\times \chi_k [2 \cos \kappa_k \\ &+ \cot \alpha \sin \kappa_k \sin(\psi_p + \zeta_k)] , \end{aligned} \quad (30)$$

$$\begin{aligned} \bar{\psi}_p^{SS} &= \frac{3\eta\pi}{\mathfrak{T} \bar{l}_r^4} \chi_1 \chi_2 \\ &\times \{ \cot \alpha [\sin \kappa_1 \cos \kappa_2 \sin(\psi_p + \zeta_1) \\ &+ \cos \kappa_1 \sin \kappa_2 \sin(\psi_p + \zeta_2)] + 2 \cos \kappa_1 \\ &\times \cos \kappa_2 - \sin \kappa_1 \sin \kappa_2 \cos(\zeta_2 - \zeta_1) \} , \end{aligned} \quad (31)$$

$$\begin{aligned} \bar{\psi}_p^{QM} &= \frac{3\eta\pi}{2\mathfrak{T} \bar{l}_r^4} \sum_{k=1}^2 \nu^{2k-3} w_k \chi_k^2 \\ &\times [\cot \alpha \sin 2\kappa_k \sin(\psi_p + \zeta_k) \\ &- 3 \sin^2 \kappa_k + 2] , \end{aligned} \quad (32)$$

$$\bar{\psi}_p^{2PN} = \frac{3\pi}{2\mathfrak{T} \bar{l}_r^4} [33\bar{e}_r^2 - 4\eta - 6\bar{e}_r^2 \eta + 2] . \quad (33)$$

All PN, spin and quadrupolar corrections lead to periastron precession.

C. Spin angles

The secular evolutions of the spin polar angles κ_i , and azimuthal angles ζ_i are:

$$\bar{\kappa}_i^{PN} = 0 , \quad (34)$$

$$\begin{aligned} \bar{\kappa}_i^{SO} &= \frac{\eta\pi}{\mathfrak{T} \bar{l}_r^3} \\ &\times (4\nu^{2j-3} + 3) \chi_j \sin \kappa_j \sin(\zeta_i - \zeta_j) , \end{aligned} \quad (35)$$

$$\begin{aligned} \bar{\kappa}_i^{SS} &= -\frac{\eta\pi}{\mathfrak{T} \bar{l}_r^4} \chi_j \sin \kappa_j \\ &\times \sin(\zeta_i - \zeta_j) (2\bar{l}_r \nu^{2j-3} + 3\chi_i \cos \kappa_i) , \end{aligned} \quad (36)$$

$$\begin{aligned} \bar{\kappa}_i^{QM} &= -\frac{3\eta\pi}{2\mathfrak{T} \bar{l}_r^4} \nu^{2j-3} w_j \chi_j^2 \\ &\times \sin 2\kappa_j \sin(\zeta_i - \zeta_j) , \end{aligned} \quad (37)$$

$$\bar{\kappa}_i^{2PN} = 0, \quad (38)$$

$$\bar{\zeta}_i^{PN} = -\bar{\psi}_p^{PN}, \quad (39)$$

$$\begin{aligned} \bar{\zeta}_i^{SO} = & \frac{\eta\pi}{\mathfrak{I} \mathfrak{I}_r^3} \{ \bar{\mathfrak{I}}_r (4 + 3\nu^{3-2i}) \\ & + 3(4\nu^{2i-3} + 3) \chi_i \cos \kappa_i + (4\nu^{2j-3} + 3) \chi_j \\ & \times [2 \cos \kappa_j + \cot \kappa_i \sin \kappa_j \cos(\zeta_i - \zeta_j)] \}, \quad (40) \end{aligned}$$

$$\begin{aligned} \bar{\zeta}_i^{SS} = & -\frac{2\eta\pi}{\mathfrak{I} \mathfrak{I}_r^3} \nu^{2j-3} \chi_j [\cos \kappa_j \\ & + \cot \kappa_i \sin \kappa_j \cos(\zeta_i - \zeta_j)] \\ & - \frac{3\eta\pi}{\mathfrak{I} \mathfrak{I}_r^4} \chi_i \chi_j \\ & \times \{ \cot \kappa_i [3 \sin \kappa_i \cos \kappa_j \\ & + \cos \kappa_i \sin \kappa_j \cos(\zeta_i - \zeta_j)] \\ & - \sin \kappa_i \sin \kappa_j \cos(\zeta_i - \zeta_j) \}, \quad (41) \end{aligned}$$

$$\begin{aligned} \bar{\zeta}_i^{QM} = & -\frac{6\eta\pi}{\mathfrak{I} \mathfrak{I}_r^3} w_i \chi_i \cos \kappa_i \\ & - \frac{3\eta\pi}{2\mathfrak{I} \mathfrak{I}_r^4} \sum_{k=1}^2 w_k \nu^{2k-3} \chi_k^2 \\ & \times [(2 - 3 \sin^2 \kappa_k) \\ & + \cot \kappa_i \sin(2\kappa_k) \cos(\zeta_i - \zeta_k)], \quad (42) \end{aligned}$$

$$\bar{\zeta}_i^{2PN} = -\bar{\psi}_p^{2PN}. \quad (43)$$

Here $i \neq j$ and $i = 1, 2$.

One of the advantages of exploring the secular dynamics is that the evolution of the spin angles decoupled from the rest of the evolutions. The evolutions for κ_i, ζ_i form a closed set of differential equations, hence it can be monitored independently.

The average of the precession angular velocities can also be computed from Eqs (31-33) of Ref. [52]. The expressions are given in Appendix D.

IV. LIMITS OF VALIDITY

A. Validity of the conservative approach: the conservative timescale

We evolve the conservative secular dynamics up to the point where the neglected 2.5PN radiation reaction term would generate an error of $p\%$, and choose the number p according to the desired accuracy. This is described with the N number of periods to evolve, when the error accumulating from neglecting the radiation reaction reaches $p\%$:

$$N = \frac{p}{100} \varepsilon^{-5/2}. \quad (44)$$

The number of periods N defines the conservative timescale. In what follows, we proceed with the choices $p = 1$ or $p = 0.1$, depending on the circumstances.

TABLE II: The coefficients L_k and K_k of $\mathfrak{I}_r(\chi_p)$.

Coefficient	Expression
L_{00}^{2PN}	$\frac{1}{96} [432e_{r0}^3\eta + e_{r0}^2(-117\eta^2 + 54\eta + 48) + 32e_{r0}(2\eta^2 - 83\eta + 50) - 48(\eta^2 - 5\eta + 6)]$
L_{10}^{2PN}	$\frac{e_{r0}}{8} [(2\eta - 33)\eta e_{r0}^2 - 116\eta^2 + 256\eta - 160]$
L_{20}^{2PN}	$\frac{1}{8} [e_{r0}^2(9\eta^2 - 3\eta - 4) + 4(\eta^2 - 5\eta + 6)]$
L_{30}^{2PN}	$\frac{e_{r0}}{24} [-3(2\eta + 3)\eta e_{r0}^2 + 32\eta^2 - 104\eta + 80]$
L_{40}^{2PN}	$\frac{3e_{r0}^2(\eta-2)\eta}{32}$
L_{01}^{2PN}	$\frac{1}{8} [e_{r0}^2(-9\eta^2 + 3\eta + 4) - 4(\eta^2 - 5\eta + 6)]$
L_{11}^{2PN}	$\frac{e_{r0}}{8} [3(2\eta + 3)\eta e_{r0}^2 - 32\eta^2 + 104\eta - 80]$
L_{21}^{2PN}	$-\frac{9e_{r0}^2(\eta-2)\eta}{16}$
L_{31}^{2PN}	0
L_{41}^{2PN}	0
L_{02}^{2PN}	$\frac{3e_{r0}^2(\eta-2)\eta}{32}$
L_{12}^{2PN}	0
L_{22}^{2PN}	0
L_{32}^{2PN}	0
L_{42}^{2PN}	0
L_0^{SS}	$2e_{r0} + 3$
L_1^{SS}	0
L_2^{SS}	-3
L_3^{SS}	$-2e_{r0}$
K_0^{SS}	$-e_{r0}$
K_1^{SS}	-3
K_2^{SS}	$-2e_{r0}$
L_0^{QM}	$-(2e_{r0} + 3)$
L_1^{QM}	0
L_2^{QM}	-3
L_3^{QM}	$-2e_{r0}$
K_0^{QM}	$-e_{r0}$
K_1^{QM}	-3
K_2^{QM}	$-2e_{r0}$

B. Accuracy of the secular dynamics on precessional timescale and above, up to the conservative timescale

We check the long-term accuracy of the secular dynamics by a numerical comparison with instantaneous dynamics, as given by Eqs. (36)-(42) of Ref. [52]. The results are represented on Figs. 1-4.

On each figure the upper block a) shows the first two

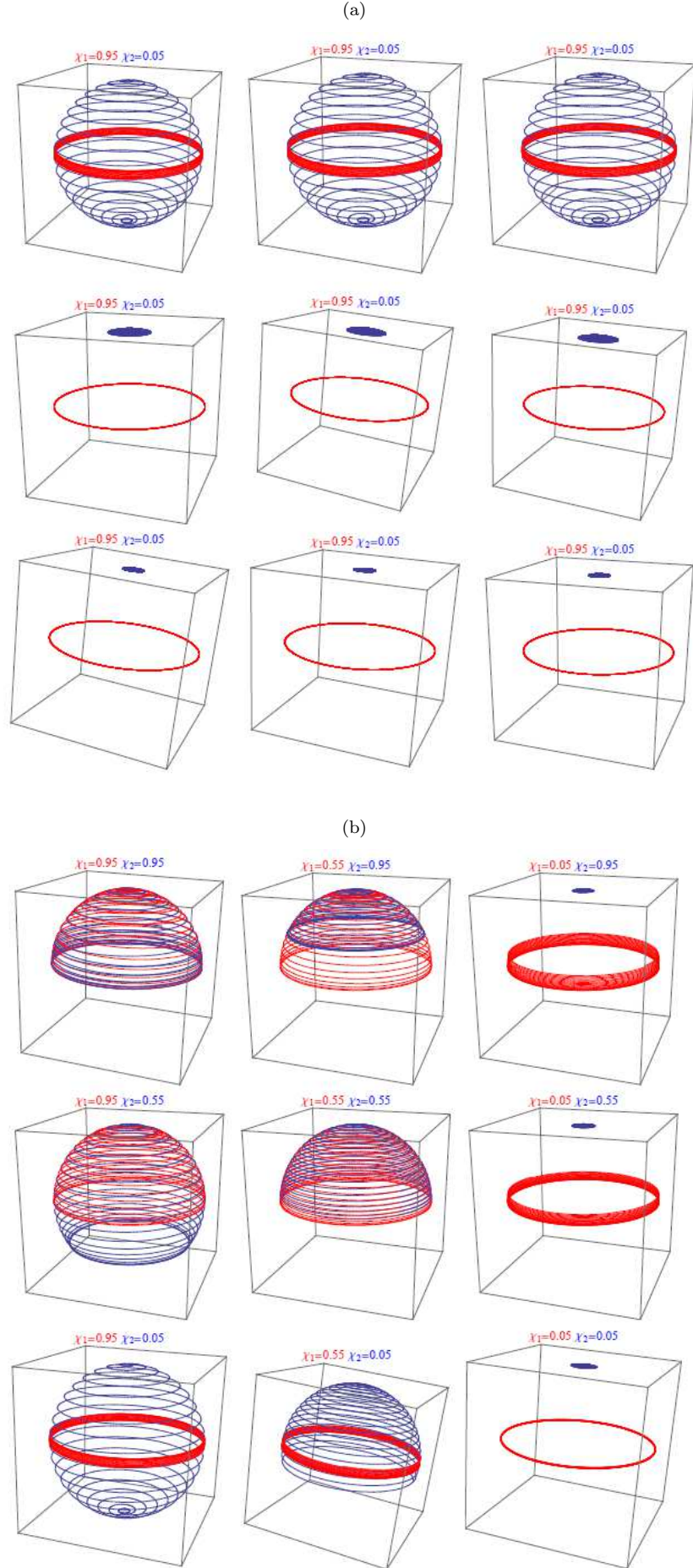


FIG. 5: The upper block a) shows the total mass and mass ratio dependence of the flip-flop. The total mass changes horizontally as $m = 100M_{\odot}, 50M_{\odot}, 10M_{\odot}$, mass ratio changes vertically as $\nu = 1.0, 0.5, 0.1$. The dimensionless spin

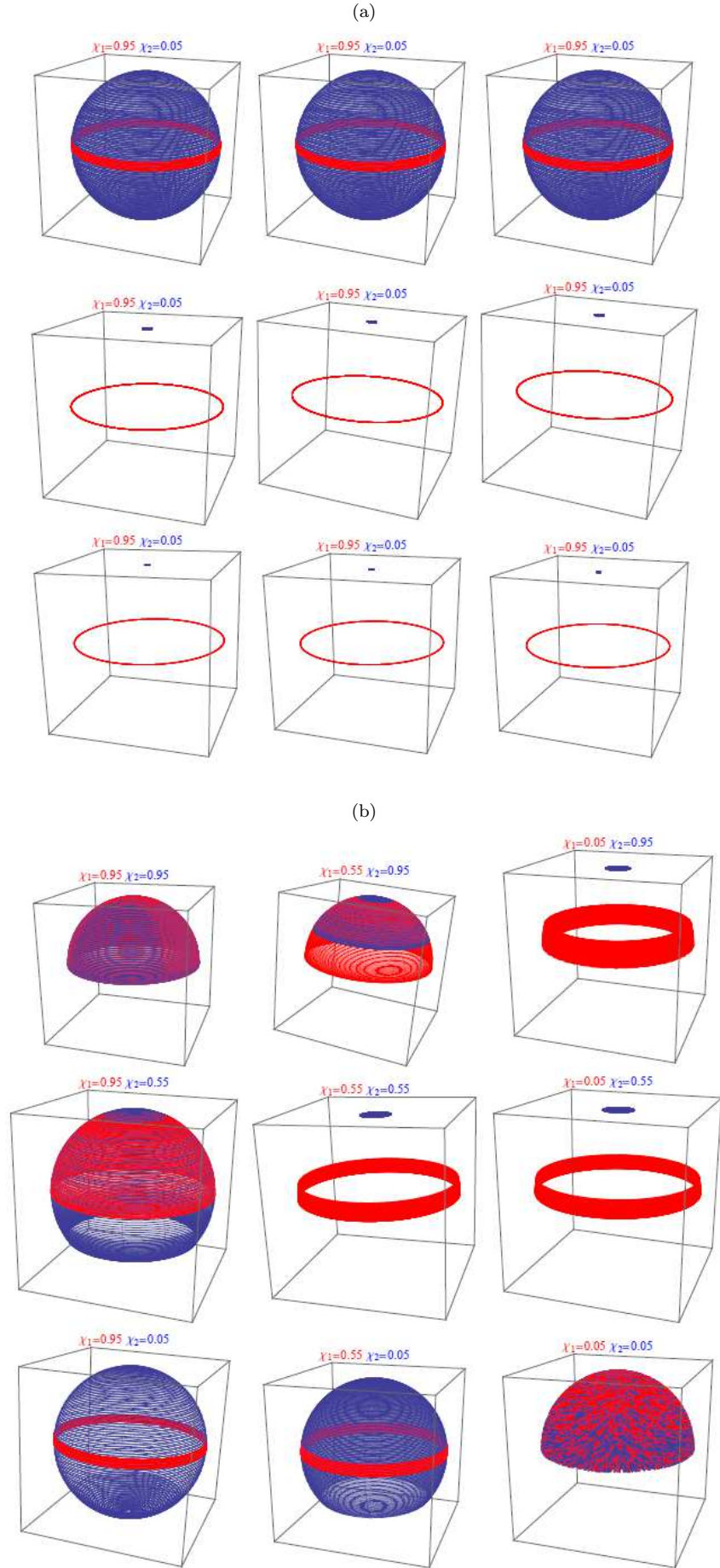


FIG. 6: The upper block a) shows the total mass and mass ratio dependence of the flip-flop. The total mass changes horizontally as $m = 100M_{\odot}, 50M_{\odot}, 10M_{\odot}$, mass ratio changes vertically as $\nu = 1.0, 0.5, 0.1$. The dimensionless spin parameters are $\chi_1 = 0.95, \chi_2 = 0.05$. The lower block b) shows the spin magnitude dependence of the flip-flop.

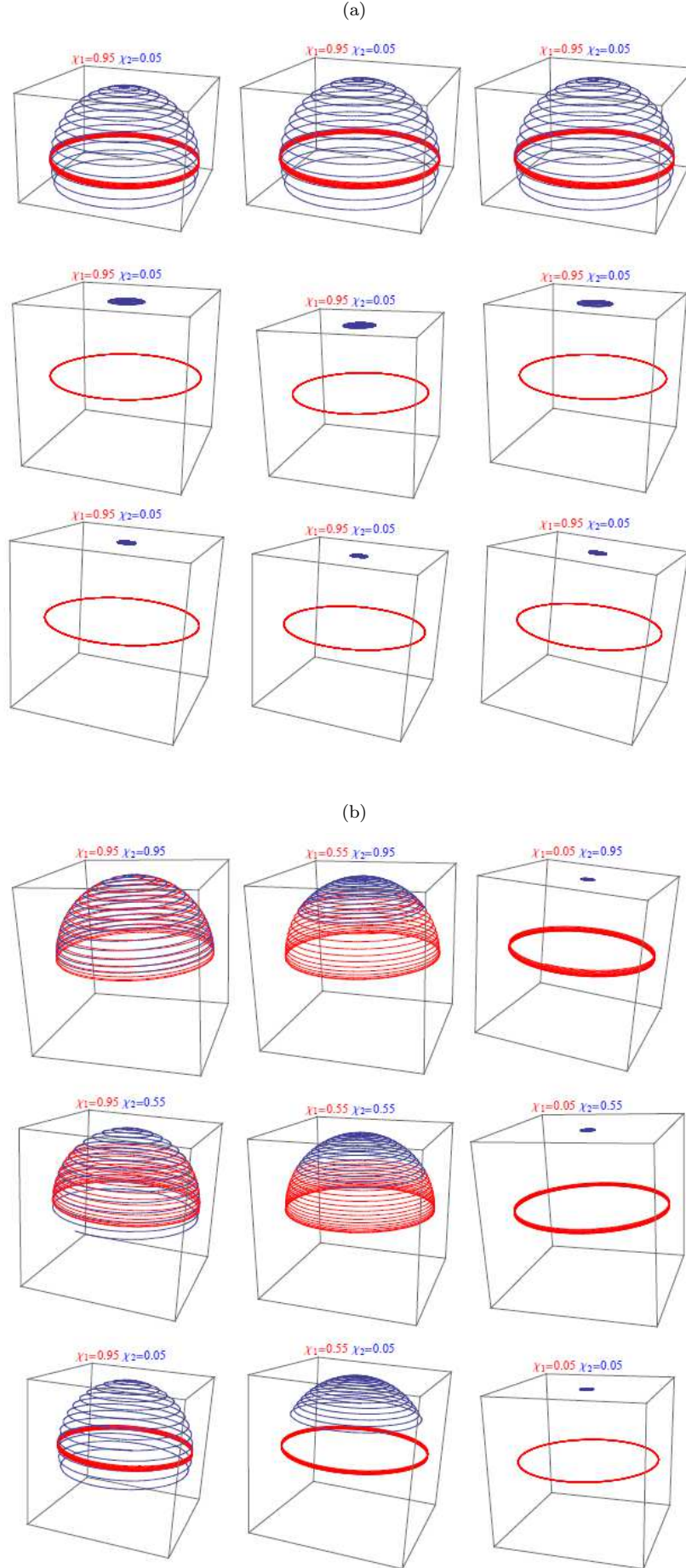


FIG. 7: The upper block a) shows the total mass and mass ratio dependence of the flip-flop. The total mass changes horizontally as $m = 100M_\odot, 50M_\odot, 10M_\odot$, mass ratio changes vertically as $\nu = 1.0, 0.5, 0.1$. The dimensionless spin parameters are $\chi_1 = 0.95$, $\chi_2 = 0.05$. The lower block b) shows the spin magnitude dependence of the flip-flop.

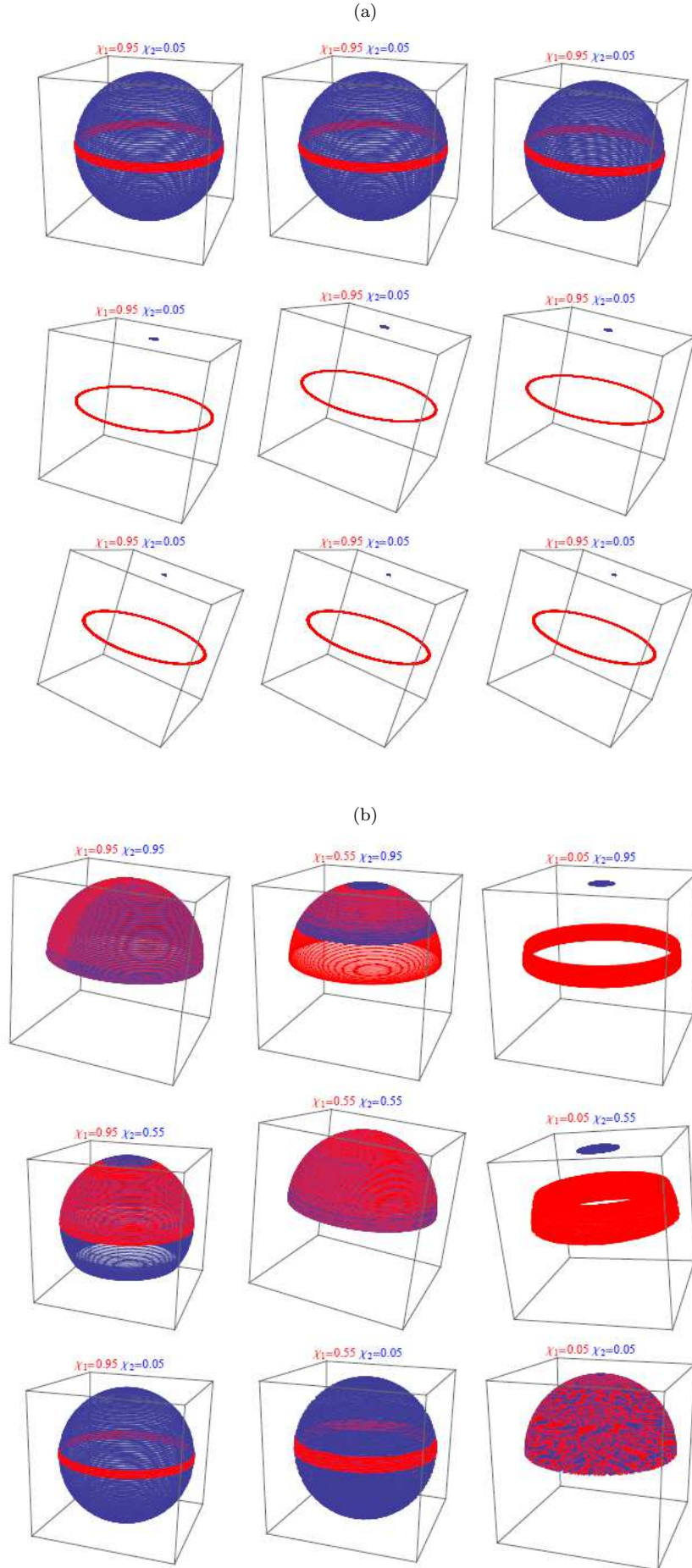


FIG. 8: The upper block a) shows the total mass and mass ratio dependence of the flip-flop. The total mass changes horizontally as $m = 100M_\odot, 50M_\odot, 10M_\odot$, mass ratio changes vertically as $\nu = 1.0, 0.5, 0.1$. The dimensionless spin parameters are $\chi_1 = 0.95, \chi_2 = 0.05$. The lower block b) shows the spin magnitude dependence of the flip-flop.

TABLE III: The PN, SS and QM coefficients E_k and F_k of e_r (χ_p).

<i>Coefficient</i>	<i>Expression</i>
E_0^{PN}	$3 - \eta + (5 - 4\eta)e_{r0} + e_{r0}^2(7 - 6\eta)$
E_1^{PN}	$-[3 - \eta + e_{r0}^2(7 - \frac{11}{2}\eta)]$
E_2^{PN}	$-(5 - 4\eta)e_{r0}$
E_3^{PN}	$\frac{\eta}{2}e_{r0}^2$
E_0^{SS}	$-\cos \kappa_1 \cos \kappa_2 (e_{r0}^2 + 3e_{r0} + 3)$ $+ \frac{1}{2} \sin \kappa_1 \sin \kappa_2 [(e_{r0}^2 + 3e_{r0} + 3) \cos \zeta_-$ $+ (7e_{r0}^2 + 15e_{r0} + 5) \cos \zeta_+]$
E_1^{SS}	$\frac{3}{2} \sin \kappa_1 \sin \kappa_2 (3 \cos \zeta_+ - \cos \zeta_-)$ $+ 3 \cos \kappa_1 \cos \kappa_2$
E_2^{SS}	$\frac{3}{2} e_{r0} \sin \kappa_1 \sin \kappa_2 (\cos \zeta_+ - \cos \zeta_-)$ $+ 3e_{r0} \cos \kappa_1 \cos \kappa_2$
E_3^{SS}	$-\frac{1}{2} e_{r0}^2 \sin \kappa_1 \sin \kappa_2 (\cos \zeta_+ + \cos \zeta_-)$ $- 7 \sin \kappa_1 \sin \kappa_2 \cos \zeta_+$ $+ e_{r0}^2 \cos \kappa_1 \cos \kappa_2$
E_4^{SS}	$-9e_{r0} \sin \kappa_1 \sin \kappa_2 \cos \zeta_+$
E_5^{SS}	$-3e_{r0}^2 \sin \kappa_1 \sin \kappa_2 \cos \zeta_+$
F_0^{SS}	$1 - e_{r0}^2$
F_1^{SS}	$-3e_{r0}$
F_2^{SS}	$-(2e_{r0}^2 + 7)$
F_3^{SS}	$-9e_{r0}$
F_4^{SS}	$-3e_{r0}^2$
E_0^{QM}	$(7e_{r0}^2 + 15e_{r0} + 5) \cos^2 \zeta_i \sin^2 \kappa_i$ $+ (2e_{r0}^2 + 3e_{r0} - 2) \cos^2 \kappa_i$ $- 3e_{r0}^2 - 6e_{r0} - 1$
E_1^{QM}	$9 \cos^2 \kappa_i \sin^2 \zeta_i + 3(3 \cos^2 \zeta_i - 2)$
E_2^{QM}	$3e_{r0}(2 - \cos^2 \zeta_i) \cos^2 \kappa_i$ $- 3e_{r0} \sin^2 \zeta_i$
E_3^{QM}	$e_{r0}^2 \cos^2 \kappa_i$ $+ [- (e_{r0}^2 + 14) \cos^2 \zeta_i + 7] \sin^2 \kappa_i$
E_4^{QM}	$-9e_{r0} \sin^2 \kappa_i \cos 2\zeta_i$
E_5^{QM}	$-3e_{r0}^2 \sin^2 \kappa_i \cos 2\zeta_i$
F_0^{QM}	$(1 - e_{r0}^2)$
F_1^{QM}	$-3e_{r0}$
F_2^{QM}	$-(2e_{r0}^2 + 7)$
F_3^{QM}	$-9e_{r0}$
F_4^{QM}	$-3e_{r0}^2$

periods of the evolution, and the lower block b) shows the evolution of the variables over the conservative timescale.

On Figs. 1 and 2 the evolution is presented for $p = 1$, thus for $N = 0.01\epsilon^{-5/2}$. On Fig. 1 the PN parameter and the eccentricity are $\epsilon = 0.01$ and $e_r = 0.1$ respectively. On Fig. 2 (as compared to Fig. 1) only the eccentricity is changed to $e_r = 0.5$. These figures show that the both spin axes are more stable for larger eccentricity. This

can be seen from the angles κ_1 , κ_2 , ζ_1 and ζ_2 on each figure's block a) within one period. Block b) also shows this over the conservative timescale. The plane of the motion changes less as shown by the angle α . The reason for this is that for lower eccentricity the compact objects stay close to each other over a larger part of the period, thus have more time to interact. This is ensured by the initial conditions being set such that at the periastron in both cases the distance between the compact objects is the same.

On Figs. 3 and 4 the evolution is presented for $p = 0.1$ only, thus for $N = 0.001\epsilon^{-5/2}$. Figs. 3 and 4 show the previous eccentricity values for the PN parameter value $\epsilon = 0.0005$. These figures exhibit the same differences for the two eccentricities. For the decrease in the PN parameter, the number of precessional periods increases over the conservative timescale. For low ϵ values long term precessional effects may be easier to identify.

V. SPIN FLIP-FLOPS

In this Section we analyse the flip-flop effect for various parameter ranges. This effect has been shown [59–61] by numerical investigations for particular configurations (equal masses, the dominant spin in the plane of motion and the smaller spin perpendicular to it) and it was claimed that to some extent it also occurs for generic mass ratios.

For our analysis we keep the specific spin orientations, but we vary the total mass, mass ratio, and spin magnitudes in each of the Figures 5-8. The z -axis is given by the Newtonian orbital angular momentum. While this direction is not conserved (the direction of the total angular momentum \mathbf{J} is) on all figures the parameters are such that \mathbf{L}_N is the dominant contribution to \mathbf{J} (the spin magnitudes are smaller than L_N). Hence the evolution is represented in a quasi-inertial system.

On all Figs. 5-8 the upper block a) shows the total mass and mass ratio dependence and the lower block b) shows the dimensionless spin magnitude dependence of the flip-flop phenomenon. For all Figs. the evolution is presented for $p = 1$. On Figs. 5 and 6 the eccentricity is set as $\bar{e}_r = 0.1$ and the PN parameter changes as $\epsilon = 0.01$ and $\epsilon = 0.0005$ respectively. On Figs. 7 and 8 the eccentricity is set as $\bar{e}_r = 0.5$ and the PN parameter changes as $\epsilon = 0.01$ and $\epsilon = 0.0005$ respectively.

The upper blocks shows that the flip-flop phenomenon slightly depends on the eccentricity. For larger eccentricity under the same time period the κ_2 angle changes less, the number of precessional period it takes for the full flip-flop to happen is larger. The reason for this is that for small eccentricity, the compact objects spend more time close to each other over one period, compared to larger eccentricities. For smaller PN parameter value however the flip-flop effect happens several times on the conservative timescale, and several full flip-flop can occur for larger eccentricities. The upper panels also show that

the effect does not depend on the total mass. The effect actually depends heavily on the mass ratio. For equal masses, the effect is prominent, however as we start to decrease the mass ratio, the effect disappears.

The lower blocks of Figs. 5-8 the effect of change in both dimensionless spin parameters χ_1 and χ_2 is shown. For equal spin magnitude values both spin angles κ_1 and κ_2 change back and forth by $\pi/2$. As we decrease the spin magnitude that closely aligns the orbital angular momentum, the flip-flop effect appears, and the larger the ratio of χ_1/χ_2 is, the more prominent the flip-flop effect is. If we change the ratio in the opposite direction the flip-flop effect completely disappears. When the ratio is 1, the aligned spin moves into the plane of the motion, and the spin initially in the plane of the motion becomes aligned with the orbital angular momentum. Then they keep changing place back and forth over the conservative timescale. The change of the PN parameter and the eccentricity has the same effect as for the total mass and mass ratio dependence.

This systematic mapping of the parameter space $(m, \nu, \chi_1, \chi_2, \varepsilon, \bar{e}_r)$ indicates that the spin flip-flop appears only at equal and co-measurable masses. The effect is too small to manifest on the conservative timescale for other parameter ranges.

VI. ORBITAL ANGULAR MOMENTUM FLIP-FLOP

The derived secular dynamics is suitable to easily monitor the evolution of the spin and orbital angular momentum vectors over several precessional cycles up to the conservative timescale. The peculiar evolution of the spins was discussed in the previous section. In this Section we give an example when the orbital angular momentum vector undergoes a similar flip-flopping behaviour. In this example the larger spin dominates over the orbital angular momentum, $L_N/S_1 \approx 0.3$. We represent the temporal evolution of \mathbf{L}_N in the system with \mathbf{J} on the z -axis. For convenience the role of time is taken by the periastron precession angle ψ_p . The venturing of the orbital angular momentum vector from pole to pole through several precession cycles is represented on Fig. 9, where the α and ψ_p angles are taken as the polar and azimuthal angle. On Fig. 10 the secular evolution of the dynamics of this particular system is shown.

VII. CONCLUDING REMARKS

In this paper we derived the conservative secular evolution of precessing compact binaries, to second post-Newtonian order accuracy, with leading-order spin-orbit, spin-spin and mass quadrupole-monopole contributions included. The secular evolution equations emerged as a closed system of first-order differential equations, which in contrast with the instantaneous dynamics, is au-

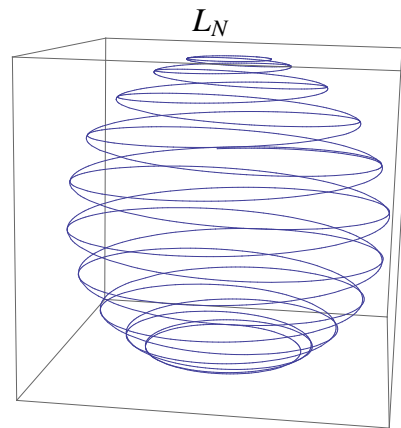


FIG. 9: The flip-flop of the orbital angular momentum with α the polar angle and ψ_p the azimuthal angle. Over several precession periods the plane of the motion flips upside down.

tonomous. The dependent variables are the polar angles of the spin vectors κ_1 and κ_2 , the azimuthal angle of the spin vectors ζ_1 and ζ_2 , the angles α and ϕ_n giving the orientation of the orbital angular momentum vector, together with the periastron angle ψ_p , the dimensionless magnitude of the orbital angular momentum l_r and the eccentricity e_r .

We proved that the secular dynamics reliably characterizes the system over the conservative timescales. The later was defined as in Eq. (44), typically larger than the precessional timescale, however shorter than the timescale of gravitational radiation. We compared the secular and instantaneous dynamics over this timescale.

The analytic equations are suitable to monitor the spin flip-flop effect, recently found by numerical relativity methods. Our investigations showed that the effect does not generalize beyond its original parameter settings: the dominant spin is in the plane of the motion, the smaller flip-flopping spin is initially closely aligned to the orbital angular momentum and the system has equal mass ratio.

We investigated the PN parameter and eccentricity dependence of the flip-flop effect on Figs 5-8. The parameters were set as $\varepsilon = 0.01, 0.0005$ and $e_r = 0.1, 0.5$. When the PN parameter decreases, the flip-flop effect occurs several times over the conservative timescale. Due to the compact objects staying together for larger part of the period for small eccentricity than for large, the frequency of the flip-flop effect is higher for small eccentricities.

As shown on the upper block a) of Figs. 5-8 the flip-flop phenomenon does not depend on the total mass, but significantly depends on the mass ratio, preferring close to equal mass systems. The lower block b) of the same Figs showed that the effect depends on the ratio of the dimensionless spin magnitudes. The effect is most prominent when the spin almost aligned with the orbital angular momentum is small, and the spin in the plane of the motion dominates. When the ratio of the spin

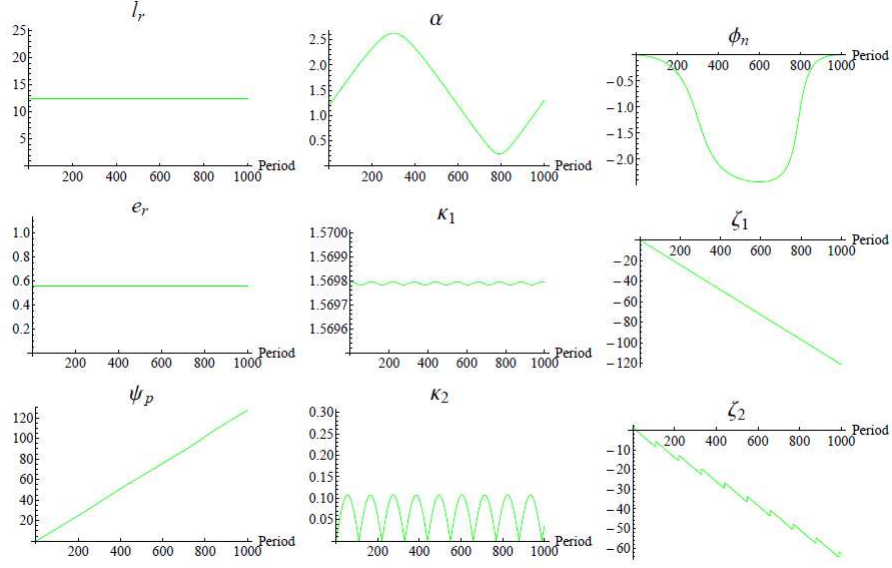


FIG. 10: The dynamics of the system where the orbital angular momentum undergoes a flip-flop like behaviour is shown over the conservative timescale with $p = 1$. The parameters for the system are as follows: total mass $m = 100M_\odot$, mass ratio $\nu = 0.03$, dimensionless spin parameters $\chi_1 = 0.95$, $\chi_2 = 0.05$. Value of the PN parameter $\varepsilon = 0.01$. Initial values of the parameters: $e_r = 0.5$, $\kappa_1 = \pi/2 - 0.001$, $\kappa_2 = 0.001$, $\zeta_1 = 0$, $\zeta_2 = \pi/2$, $\psi_p = 0$, $\phi_n = 0$.

magnitudes is 1, both spins do a half flip-flop over the conservative timescale.

In addition, a similar evolution of the orbital angular momentum vector was found, which ventures from one pole to another through several precessional periods. For this phenomenon to occur the larger spin has to dominate over the orbital angular momentum. In our investigation we found the effect for the ratio $L_N/S_1 \approx 0.3$. This can only be achieved with small mass ratios $\nu \ll 1$ during the inspiral.

VIII. ACKNOWLEDGEMENTS

In the early stages of this work L. Á. G. was supported by the European Union and the State of Hungary, co-financed by the European Social Fund in the framework of TÁMOP 4.2.4. A/2-11/-1-2012-0001 “National Excellence Program.”

Appendix A: The χ_p dependent shape variables and the period

We derive the χ_p dependence of the dimensionless orbital angular momentum $\mathfrak{l}_r(\chi_p)$ and the dimensionless orbital eccentricity $e_r(\chi_p)$. A lower index 0 indicates values taken at $\chi_p = 0$.

$$\mathfrak{l}_r(\chi_p = 0) = \mathfrak{l}_{r0}, \quad (\text{A1})$$

$$e_r(\chi_p = 0) = e_{r0}. \quad (\text{A2})$$

With $\dot{\chi}_p$ containing Newtonian order terms, to calculate the period to 2PN order, the χ_p dependence of $\mathfrak{l}_r(\chi_p)$ and of $e_r(\chi_p)$ has to be taken into account up to 2PN order. The rest of the orbital elements ψ_p , α , ϕ_n , and spin angles κ_i , ζ_i ($i = 1, 2$) do not enter at Newtonian order, hence for the 2PN calculations, only their leading order expressions are needed, which are constant.

1. The χ_p dependence of \mathfrak{l}_r

Formal integration of Eqs. (36) of Ref. [52] by exploring it's Eq. (43) gives

$$\begin{aligned} \mathfrak{l}_r(\chi_p) &= \mathfrak{l}_{r0} + \int_0^{\chi_p} \frac{\dot{\mathfrak{l}}_r}{\dot{\chi}_p} d\chi_p \\ &= \mathfrak{l}_{r0} + \frac{1}{\mathfrak{l}_{r0}} \mathfrak{l}_{rPN}(\chi_p) + \frac{1}{\mathfrak{l}_{r0}^2} \mathfrak{l}_{rSO}(\chi_p) \\ &\quad + \frac{1}{\mathfrak{l}_{r0}^3} \mathfrak{l}_{rQM}(\chi_p) + \frac{1}{\mathfrak{l}_{r0}^3} \mathfrak{l}_{rSS}(\chi_p) \\ &\quad + \frac{1}{\mathfrak{l}_{r0}^3} \mathfrak{l}_{r2PN}(\chi_p), \end{aligned} \quad (\text{A3})$$

with

$$\mathfrak{l}_{rPN}(\chi_p) = 2(2 - \eta) e_{r0} (1 - \cos \chi_p), \quad (\text{A4})$$

$$\mathfrak{l}_{r2PN}(\chi_p) = \sum_{k=0}^4 \sum_{l=0}^2 L_{kl}^{2PN} \sin^{2l} \chi_p \cos^k \chi_p, \quad (\text{A5})$$

$$\begin{aligned} \mathfrak{l}_{rSO}(\chi_p) &= -\frac{\eta e_{r0}}{2} (\cos \chi_p - 1) \\ &\times \sum_{k=1}^2 (4^{2k-3} + 3) \chi_k \cos \kappa_k, \quad (\text{A6}) \end{aligned}$$

$$\begin{aligned} \mathfrak{l}_{rSS}(\chi_p) &= \eta \chi_1 \chi_2 \sin \kappa_1 \sin \kappa_2 \\ &\times \left[\cos \zeta_+ \sum_{k=0}^3 L_k^{SS} \cos^k \chi_p \right. \\ &\left. + \sin \zeta_+ \sin \chi_p \sum_{k=0}^2 K_k^{SS} \cos^k \chi_p \right], \quad (\text{A7}) \end{aligned}$$

$$\begin{aligned} \mathfrak{l}_{rQM}(\chi_p) &= \frac{\eta}{2} \sum_{i=1}^2 \chi_i^2 w_i \nu^{2i-3} \sin^2 \kappa_i \\ &\times \left[\cos 2\zeta_i \sum_{k=0}^3 L_k^{QM} \cos^k \chi_p \right. \\ &\left. + \sin 2\zeta_i \sin \chi_p \sum_{k=0}^2 K_k^{QM} \cos^k \chi_p \right] \quad (\text{A8}) \end{aligned}$$

where the coefficients L_k and K_k of $\mathfrak{l}_r(\chi_p)$ are shown in Table II.

2. The χ_p dependence of e_r

Formal integration of Eqs. (37) of Ref. [52] by exploring its Eq. (43) leads to

$$\begin{aligned} e_r(\chi_p) &= e_{r0} + \int_0^{\chi_p} \frac{\dot{e}_r}{\dot{\chi}_p} d\chi_p = \\ &= e_{r0} + \frac{1}{\mathfrak{l}_{r0}^2} e_{rPN}(\chi_p) + \frac{1}{\mathfrak{l}_{r0}^3} e_{rSO}(\chi_p) \\ &\quad + \frac{1}{\mathfrak{l}_{r0}^4} e_{rQM}(\chi_p) + \frac{1}{\mathfrak{l}_{r0}^4} e_{rSS}(\chi_p) \\ &\quad + \frac{1}{\mathfrak{l}_{r0}^4} e_{r2PN}(\chi_p), \quad (\text{A9}) \end{aligned}$$

with

$$e_{rPN}(\chi_p) = \sum_{k=0}^3 E_k^{PN} \cos^k \chi_p, \quad (\text{A10})$$

$$\begin{aligned} e_{rSO}(\chi_p) &= \frac{\eta}{2} (1 - e_{r0}^2) (1 - \cos \chi_p) \times \\ &\times \sum_{i=1}^2 (4^{2i-3} + 3) \chi_i \cos \kappa_i, \quad (\text{A11}) \end{aligned}$$

$$\begin{aligned} e_{rSS}(\chi_p) &= \eta \chi_1 \chi_2 \left[\sum_{k=0}^5 E_k^{SS} \cos^k \chi_p \right. \\ &\left. + \sin \kappa_1 \sin \kappa_2 \sin \zeta_+ \sin \chi_p \sum_{k=0}^4 F_k^{SS} \cos^k \chi_p \right], \quad (\text{A12}) \end{aligned}$$

$$\begin{aligned} e_{rQM}(\chi_p) &= \frac{\eta}{2} \sum_{i=1}^2 \chi_i^2 \nu^{2i-3} w_i \\ &\times \left[\sum_{k=0}^6 E_k^{QM} \cos^k \chi_p \right. \\ &\left. + \sin 2\zeta_i \sin^2 \kappa_i \sin \chi_p \right. \\ &\left. \times \sum_{k=0}^4 F_k^{QM} \cos^k \chi_p \right], \quad (\text{A13}) \end{aligned}$$

The coefficients E_k and F_k of $e_r(\chi_p)$ for the PN, SS and QM contributions are shown in Table III.

$$e_{r2PN}(\chi_p) = \sum_{l=0}^3 \sum_{k=0}^6 E_{kl}^{2PN} \cos^k \chi_p \sin^{2l} \chi_p. \quad (\text{A14})$$

The coefficients E_k^{2PN} and F_k^{2PN} of $e_r(\chi_p)$ are shown in Table IV.

3. Dimensionless 2PN radial period

Everything required to calculate the 2PN radial period is given now. We insert the expressions of $\mathfrak{l}_r(\chi_p)$ and $e_r(\chi_p)$ into the integral (3) and Taylor-expand to 2PN order. The various contributions to the period (4) read as

$$\mathfrak{T}_0 = \frac{2\pi \mathfrak{l}_{r0}^3}{(1 - e_{r0}^2)^{3/2}}, \quad (\text{A15})$$

$$\tau_{01PN} = -\frac{(1 - e_{r0}^2) (e_{r0}^2(7\eta - 6) + 2e_{r0}(5\eta - 3) + 4\eta - 18)}{2(e_{r0} - 1)^2},$$

$$\tau_{0SO} = 0, \quad (\text{A16})$$

$$\begin{aligned} \tau_{02PN} &= \frac{1}{40(1 - e_{r0})^2 e_{r0}^4} \left[\sum_{k=0}^{10} U_k e_{r0}^k \right. \\ &\quad \left. - \frac{(1 - e_{r0}^2)^{3/2}}{2(1 - e_{r0})} \sum_{k=0}^7 V_k e_{r0}^k \right], \quad (\text{A17}) \end{aligned}$$

$$\begin{aligned} \tau_{0SS} &= -\frac{3\chi_1 \chi_2 (1 + e_{r0})^2 \eta}{(1 - e_{r0}) \mathfrak{l}_{r0}^4} [\cos \kappa_1 \cos \kappa_2 + \sin \kappa_1 \sin \kappa_2 \\ &\quad \times (\sin \zeta_1 \sin \zeta_2 - 2 \cos \zeta_1 \cos \zeta_2)], \quad (\text{A18}) \end{aligned}$$

$$\begin{aligned} \tau_{0QM} &= -\frac{3\eta (1 + e_{r0})^2}{2(1 - e_{r0}) \mathfrak{l}_{r0}^4} \sum_{i=1}^2 \chi_i^2 \nu^{2i-3} w_i \\ &\quad \times (1 - 3 \sin^2 \kappa_i \cos^2 \zeta_i). \quad (\text{A19}) \end{aligned}$$

The coefficients U_k and V_k of τ_{02PN} are enlisted in Table V.

Appendix B: The secular shape variables \bar{l} and \bar{e}_r

We calculate the secular shape variables. For \bar{l}_r we compute the integral given in Eq. (13). We get

$$\bar{l}_{rN} = \frac{2\pi l_{r0}^4}{(1 - e_{r0}^2)^{3/2}}, \quad (B1)$$

$$\bar{l}_{rPN} = -\frac{\pi l_{r0}^2}{(1 - e_{r0})^2 \sqrt{1 - e_{r0}^2}} [e_{r0}^2 (3\eta + 2) + 14e_{r0}(\eta - 1) + 4\eta - 18], \quad (B2)$$

$$\bar{l}_{rSO} = -\frac{\pi e_{r0} \eta l_{r0}}{(1 - e_{r0}) \sqrt{1 - e_{r0}^2}} \times \sum_{k=1}^2 (4^{2k-3} + 3) \chi_k \cos \kappa_k, \quad (B3)$$

$$\bar{l}_{r2PN} = \frac{\pi}{120e_{r0}^4} \sum_{k=0}^4 \bar{L}_k^{2PN} e_{r0}^k - \frac{\pi \sqrt{1 - e_{r0}^2}}{60(e_{r0} - 1)^4 e_{r0}^4} \sum_{k=0}^8 \bar{K}_k^{2PN} e_{r0}^k, \quad (B4)$$

$$\bar{l}_{rSS} = \frac{\pi \chi_1 \chi_2 \eta}{16(1 - e_{r0}) e_{r0}^2 (1 - e_{r0}^2)^{3/2}} \times (\cos \kappa_1 \cos \kappa_2 \bar{L}^{SS} + \sin \kappa_1 \sin \kappa_2 \bar{K}^{SS}), \quad (B5)$$

$$\bar{l}_{rQM} = \frac{\pi (e_{r0}^2 + 2) \eta}{256e_{r0} (1 - e_{r0}^2)^{5/2}} \sum_{k=1}^2 \chi_k^2 \nu^{2k-3} w_k \times [-4(47e_{r0}^3 + 1050e_{r0}^2 + 488e_{r0} + 480) \sin^2 \kappa_k \cos 2\zeta_k + 16(5e_{r0}^3 + 21e_{r0}^2 + 15e_{r0} + 6) \times (3 \cos 2\kappa_k + 1)]. \quad (B6)$$

Here the coefficients \bar{L}_k and \bar{K}_k of \bar{l}_r are shown in Table VI.

For \bar{e}_r we compute the integral given in Eq. (14). We get

$$\bar{e}_{rN} = \frac{2\pi e_{r0} l_{r0}^3}{(1 - e_{r0}^2)^{3/2}}, \quad (B7)$$

$$\bar{e}_{rPN} = \frac{\pi l_{r0}}{e_{r0}} \{2(3\eta - 5) + \frac{\sqrt{1 - e_{r0}^2}}{(1 - e_{r0})^3 (e_{r0} + 1)} [4e_{r0}^4 (\eta - 2) - 20e_{r0}^3 (\eta - 1) + e_{r0}^2 (22 - 9\eta) + 2e_{r0} (5\eta - 7) - 6\eta + 10]\}, \quad (B8)$$

$$\bar{e}_{rSO} = \frac{\pi (e_{r0} + 1) \eta}{\sqrt{1 - e_{r0}^2}} \times \sum_{k=1}^2 (4^{2k-3} + 3) \chi_k \cos \kappa_k, \quad (B9)$$

$$\bar{e}_{r2PN} = \frac{\pi}{480e_{r0}^3 l_{r0}} \sum_{k=0}^4 \bar{E}_k^{2PN} e_{r0}^k - \frac{\pi \sqrt{1 - e_{r0}^2}}{60(e_{r0} - 1)^4 e_{r0}^3 l_{r0}} \sum_{k=0}^8 \bar{F}_k^{2PN} e_{r0}^k, \quad (B10)$$

$$\bar{e}_{rSS} = \frac{3\pi \chi_1 \chi_2 \eta}{16(1 - e_{r0}) e_{r0}^3 (1 - e_{r0}^2)^2 l_{r0}} \times (\cos \kappa_1 \cos \kappa_2 \bar{E}^{SS} + \sin \kappa_1 \sin \kappa_2 \bar{F}^{SS}), \quad (B11)$$

$$\bar{e}_{rQM} = \frac{\pi (e_{r0}^2 + 2) \eta}{128(1 - e_{r0}^2)^{5/2} l_{r0}} \sum_{k=1}^2 \chi_k^2 \nu^{2k-3} w_k \times [-4(10e_{r0}^3 + 609e_{r0}^2 + 260e_{r0} + 336) \sin^2 \kappa_k \cos 2\zeta_k + 8(4e_{r0}^3 + 27e_{r0}^2 + 15e_{r0} + 12) \times (3 \cos 2\kappa_k + 1)]. \quad (B12)$$

Here the coefficients \bar{E}_k and \bar{F}_k of \bar{e}_r are shown in Table VII.

Appendix C: Expressing the shape variables at $\chi_p = 0$ in terms of the averaged quantities \bar{l} and \bar{e}_r

In this subsection we invert Eqs. (15) and (16) in terms of \bar{l} and \bar{e}_r . We need two steps, the first is taking the perturbations to first order. Using Eqs (15), (B1) and (A15) for l_{r0} we get

$$l_{r0} = \bar{l}_r \frac{\mathfrak{T}}{\mathfrak{T}_0} - \frac{1}{\mathfrak{T}_0} (\bar{l}_{rPN} + \bar{l}_{rSO} + \bar{l}_{rSS} + \bar{l}_{rQM}). \quad (C1)$$

Using Eqs (16), (B7) and (A15) for e_{r0} we get

$$e_{r0} = \bar{e}_r \frac{\mathfrak{T}}{\mathfrak{T}_0} - \frac{1}{\mathfrak{T}_0} (\bar{e}_{rPN} + \bar{e}_{rSO} + \bar{e}_{rSS} + \bar{e}_{rQM}), \quad (C2)$$

In the perturbation terms we have to insert the leading order terms of l_{r0} and e_{r0}

$$l_{r0} = \bar{l}_r, \quad (C3)$$

$$e_{r0} = \bar{e}_r. \quad (C4)$$

The results are as follows:

$$\mathfrak{l}_{r0PN} = \frac{2\bar{e}_r(\bar{e}_r + 1)(\eta - 2)}{\bar{\mathfrak{l}}_r}, \quad (\text{C5})$$

$$\begin{aligned} \mathfrak{l}_{r0SO} = & -\frac{\bar{e}_r(1 - \bar{e}_r^2)\eta}{2(\bar{e}_r - 1)\bar{\mathfrak{l}}_r^2} \\ & \times \sum_{k=1}^2 (4^{2k-3} + 3) \chi_k \cos \kappa_k, \end{aligned} \quad (\text{C6})$$

$$\begin{aligned} \mathfrak{l}_{r0SS} = & -\frac{\chi_1 \chi_2 \eta}{32(1 - \bar{e}_r)\bar{e}_r^2 \bar{\mathfrak{l}}_r^3} (L_0^{SS} \cos \kappa_1 \cos \kappa_2 \\ & - K_0^{SS} \sin \kappa_1 \sin \kappa_2), \end{aligned} \quad (\text{C7})$$

$$\begin{aligned} \mathfrak{l}_{r0QM} = & \frac{\eta}{512\bar{e}_r(\bar{e}_r^2 - 1)\bar{\mathfrak{l}}_r^3} \sum_{k=1}^2 \chi_k^2 \nu^{2k-3} w_k \\ & \times [-4(47\bar{e}_r^5 + 1338\bar{e}_r^4 + 1446\bar{e}_r^3 \\ & + 3444\bar{e}_r^2 + 1264\bar{e}_r + 960) \\ & \times \sin^2 \kappa_k \cos 2\zeta_k + 16(5\bar{e}_r^5 + 33\bar{e}_r^4 \\ & + 61\bar{e}_r^3 + 84\bar{e}_r^2 + 42\bar{e}_r + 12) \\ & \times (3 \cos 2\kappa_k + 1)], \end{aligned} \quad (\text{C8})$$

where the coefficients L_0 and K_0 can be found in Table VIII. For e_{r0} we get

$$\begin{aligned} e_{r0PN} = & \frac{1}{\bar{e}_r \bar{\mathfrak{l}}_r^2} \left\{ - (1 - \bar{e}_r^2)^{3/2} (3\eta - 5) \right. \\ & + \frac{(1 + \bar{e}_r)^2}{2} [\bar{e}_r^2 (11\eta - 14) \\ & \left. - 2\bar{e}_r (5\eta - 7) + 6\eta - 10] \right\}, \end{aligned}$$

$$\begin{aligned} e_{r0SO} = & -\frac{(\bar{e}_r + 1)(1 - \bar{e}_r^2)\eta}{2\bar{\mathfrak{l}}_r^3} \\ & \times \sum_{k=1}^2 (4^{2k-3} + 3) \chi_k \cos \kappa_k, \end{aligned}$$

$$\begin{aligned} e_{r0SS} = & -\frac{3\chi_1 \chi_2 \eta}{32(1 - \bar{e}_r)\bar{e}_r^3 \bar{\mathfrak{l}}_r^4} (E_0^{SS} \cos \kappa_1 \cos \kappa_2 \\ & - F_0^{SS} \sin \kappa_1 \sin \kappa_2), \end{aligned} \quad (\text{C9})$$

$$\begin{aligned} e_{r0QM} = & \frac{\eta}{256(\bar{e}_r^2 - 1)\bar{\mathfrak{l}}_r^4} \sum_{k=1}^2 \chi_k^2 \nu^{2k-3} w_k \\ & \times [-4(10\bar{e}_r^5 + 753\bar{e}_r^4 + 712\bar{e}_r^3 \\ & + 1986\bar{e}_r^2 + 664\bar{e}_r + 672) \\ & \times \sin^2 \kappa_k \cos 2\zeta_k + 8(4\bar{e}_r^5 + 39\bar{e}_r^4 \\ & + 59\bar{e}_r^3 + 102\bar{e}_r^2 + 42\bar{e}_r \\ & + 24)(3 \cos 2\kappa_k + 1)]. \end{aligned} \quad (\text{C10})$$

where the coefficients L_0 and K_0 can be found in Table IX.

The second step is to derive the 2PN terms. For this we have to use the same equations as in the first step: Eqs (15), (B1) and (A15) for \mathfrak{l}_{r0} and Eqs (16), (B7) and (A15) for e_{r0}

$$\mathfrak{l}_{r0} = \bar{\mathfrak{l}}_r \frac{\mathfrak{T}}{\mathfrak{T}_0} - \frac{1}{\mathfrak{T}_0} (\bar{\mathfrak{l}}_{rPN} + \bar{\mathfrak{l}}_{r2PN}), \quad (\text{C11})$$

$$e_{r0} = \bar{e}_r \frac{\mathfrak{T}}{\mathfrak{T}_0} - \frac{1}{\mathfrak{T}_0} (\bar{e}_{rPN} + \bar{e}_{r2PN}). \quad (\text{C12})$$

This time, in order to get the 2PN terms we need the previously calculated 1PN expressions of \mathfrak{l}_{r0} and e_{r0} . After Taylor-expanding to 2PN order we get .

$$\begin{aligned} \mathfrak{l}_{r02PN} = & -\frac{(1 - \bar{e}_r^2)^{3/2}}{24\bar{e}_r^2 \bar{\mathfrak{l}}_r^3} \sum_{k=0}^2 L_{0,k}^{2PN} \bar{e}_r^k \\ & + \frac{(\bar{e}_r + 1)^2}{12\bar{e}_r^2 \bar{\mathfrak{l}}_r^3} \sum_{k=0}^4 K_{0,k}^{2PN} \bar{e}_r^k, \end{aligned} \quad (\text{C13})$$

$$\begin{aligned} e_{r02PN} = & -\frac{(1 - \bar{e}_r^2)^{3/2}}{960\bar{e}_r^3 \bar{\mathfrak{l}}_r^4} \sum_{k=0}^4 E_{0,k}^{2PN} \bar{e}_r^k \\ & + \frac{(1 + \bar{e}_r)^2}{120\bar{e}_r^3 \bar{\mathfrak{l}}_r^4} \sum_{k=0}^6 F_{0,k}^{2PN} \bar{e}_r^k. \end{aligned} \quad (\text{C14})$$

The coefficients L_0^{2PN} and K_0^{2PN} are given in Table VIII, while the terms E_0^{2PN} and F_0^{2PN} can be found in Table IX.

Appendix D: Secular precession angular velocities

The averaged precession angular velocities are calculated from Eqs (31-33) of Ref. [52]¹.

$$\begin{aligned} \overline{\omega_{\mathbf{i}} \cdot \hat{\mathbf{A}}_{\mathbf{N}}} = & \frac{2\eta\pi}{\mathfrak{T} \bar{\mathfrak{l}}_r^3} (\nu^{2j-3} \chi_j \sin \kappa_j \cos \zeta_j \\ & + 3w_i \chi_i \sin \kappa_i \cos \zeta_i) \end{aligned} \quad (\text{D1})$$

$$\begin{aligned} \overline{\omega_{\mathbf{i}} \cdot \hat{\mathbf{Q}}_{\mathbf{N}}} = & \frac{2\eta\pi}{\mathfrak{T} \bar{\mathfrak{l}}_r^3} (\nu^{2j-3} \chi_j \sin \kappa_j \sin \zeta_j \\ & + 3w_i \chi_i \sin \kappa_i \sin \zeta_i) \end{aligned} \quad (\text{D2})$$

¹ In the equations (B34) of Ref. [51] the SS and QM terms have typos: the 1/2 factors should be removed. We thank Krisztina Kövér for pointing this out to us. Due to this, Eqs. (31), (32) and the second term of Eq. (33) of Ref. [52] contain unnecessary 1/2 factors on the rhs (but otherwise all conclusions remain unchanged). In the present paper these have been corrected and both the instantaneous and secular dynamics are represented correctly.

$$\overline{\omega_{\mathbf{i}} \cdot \hat{\mathbf{L}}_{\mathbf{N}}} = \frac{\eta\pi}{\mathfrak{T} \bar{l}_r^3} \left[\bar{l}_r (4 + 3\nu^{3-2i}) + 2\nu^{2j-3} \chi_j \cos \kappa_j \right] \quad (\text{D3})$$

It is easy to see by checking the leading order term of \mathfrak{T} that as \bar{e}_r goes to 1 the precession becomes increasingly small. It is explained by the fact that on parabolic orbits, when $e_r = 1$, the motion becomes unbound, and there is no well defined period, thus no precession.

TABLE IV: The coefficients E_k^{2PN} and F_k^{2PN} of $e_r(\chi_p)$.

<i>Coefficient</i>	<i>Expression</i>
E_{00}^{2PN}	$\frac{1}{1920e_{r0}} [1920e_{r0}^5\eta(3\eta + 8) + e_{r0}^4(-1845\eta^2 + 8880\eta + 1800) + 32e_{r0}^3(232\eta^2 - 2825\eta + 1740) - 180e_{r0}^2(29\eta^2 + 89\eta + 60) + 160e_{r0}(8\eta^2 - 187\eta - 60) - 480(\eta - 3)^2]$
E_{10}^{2PN}	$-\frac{1}{64} [e_{r0}^4\eta(161\eta + 477) + 4e_{r0}^2(136\eta^2 - 849\eta + 564) + 16\eta(8\eta - 85)]$
E_{20}^{2PN}	$\frac{1}{256e_{r0}} [e_{r0}^4(269\eta^2 - 1312\eta - 256) + 32e_{r0}^2(5\eta^2 + 109\eta + 20) + 64(\eta - 3)^2]$
E_{30}^{2PN}	$\frac{1}{384} [-3e_{r0}^4\eta(53\eta + 73) + 8e_{r0}^2(208\eta^2 - 269\eta + 300) + 128(4\eta^2 - 17\eta + 15)]$
E_{40}^{2PN}	$\frac{e_{r0}}{128} [e_{r0}^2(-13\eta^2 + 64\eta + 8) + 268\eta^2 - 676\eta + 400]$
E_{50}^{2PN}	$-\frac{3e_{r0}^2\eta}{640} [5e_{r0}^2(3\eta - 1) - 64\eta + 80]$
E_{60}^{2PN}	$\frac{3e_{r0}^3\eta^2}{256}$
E_{01}^{2PN}	$-E_{20}^{2PN}$
E_{11}^{2PN}	$-3E_{30}^{2PN}$
E_{21}^{2PN}	$-\frac{3}{2}E_{40}^{2PN}$
E_{31}^{2PN}	$-\frac{1}{10}E_{50}^{2PN}$
E_{41}^{2PN}	$-9E_{60}^{2PN}$
E_{51}^{2PN}	0
E_{61}^{2PN}	0
E_{02}^{2PN}	E_{40}^{2PN}
E_{12}^{2PN}	$\frac{1}{5}E_{50}^{2PN}$
E_{22}^{2PN}	$9E_{60}^{2PN}$
E_{32}^{2PN}	0
E_{42}^{2PN}	0
E_{52}^{2PN}	0
E_{62}^{2PN}	0
E_{03}^{2PN}	$-E_{60}^{2PN}$
E_{13}^{2PN}	0
E_{23}^{2PN}	0
E_{33}^{2PN}	0
E_{43}^{2PN}	0
E_{53}^{2PN}	0
E_{63}^{2PN}	0

TABLE V: The coefficients U_k and V_k of τ_{02PN} .

<i>Coefficient</i>	<i>Expression</i>
U_{10}	$-105(\eta + 1)\eta$
U_9	$10(-559\eta + 297\eta^2 + 228)$
U_8	$5(-2674\eta + 1289\eta^2 + 1336)$
U_7	$-4(-235\eta + 186\eta^2 - 280)$
U_6	$-482\eta^2 + 25\eta + 1120$
U_5	$2(-17245\eta + 5496\eta^2 + 12200)$
U_4	$2(-2240\eta + 79\eta^2 + 3350)$
U_3	$-4(-7075\eta + 2137\eta^2 + 5300)$
U_2	$2(-3915\eta + 1317\eta^2 + 2050)$
U_1	$40(-254\eta + 67\eta^2 + 210)$
U_0	$-20(-238\eta + 65\eta^2 + 180)$
V_7	$5(-932\eta + 509\eta^2 + 504)$
V_6	$-5(-2700\eta + 1399\eta^2 + 1352)$
V_5	$1427\eta^2 + 920\eta - 4240$
V_4	$12079\eta^2 - 35880\eta + 25680$
V_3	$-4(-6875\eta + 2606\eta^2 + 3650)$
V_2	$-4(-4735\eta + 998\eta^2 + 4850)$
V_1	$40(-746\eta + 199\eta^2 + 600)$
V_0	$-40(-238\eta + 65\eta^2 + 180)$

TABLE VI: The coefficients \bar{L}_k and \bar{K}_k of \bar{l}_r .

<i>Coefficient</i>	<i>Expression</i>
\bar{L}_4^{2PN}	$15(467\eta^2 - 580\eta + 296)$
\bar{L}_3^{2PN}	$480(4\eta^2 - 3\eta + 5)$
\bar{L}_2^{2PN}	$-4(3001\eta^2 - 9445\eta + 6610)$
\bar{L}_1^{2PN}	$-480(\eta^2 - 8\eta + 15)$
\bar{L}_0^{2PN}	$120(65\eta^2 - 238\eta + 180)$
\bar{K}_8^{2PN}	$15\eta(29\eta - 3)$
\bar{K}_7^{2PN}	$-60(129\eta^2 - 188\eta + 74)$
\bar{K}_6^{2PN}	$-15(116\eta^2 - 711\eta + 304)$
\bar{K}_5^{2PN}	$2(5516\eta^2 - 15155\eta + 5420)$
\bar{K}_4^{2PN}	$-4(5347\eta^2 - 13720\eta + 6400)$
\bar{K}_3^{2PN}	$8(\eta^2 + 2735\eta - 4265)$
\bar{K}_2^{2PN}	$20308\eta^2 - 81610\eta + 71380$
\bar{K}_1^{2PN}	$-720(22\eta^2 - 82\eta + 65)$
\bar{K}_0^{2PN}	$60(65\eta^2 - 238\eta + 180)$
\bar{L}^{SS}	$4e_{r0}(4e_{r0}^4 + 29e_{r0}^3 + 30e_{r0}^2 + 48e_{r0} + 24)$
\bar{K}^{SS}	$\cos(\zeta_1 + \zeta_2)[96e_{r0}^3 - 236e_{r0}^2 - 171e_{r0}^4 + 95e_{r0}^5 + 56e_{r0} - 32 - 32\sqrt{1 - e_{r0}^2}(e_{r0}^2 - e_{r0}^3 + e_{r0} - 1)]$ $-2e_{r0}\cos(\zeta_1 - \zeta_2)(4e_{r0}^4 + 29e_{r0}^3 + 30e_{r0}^2 + 48e_{r0} + 24)$

TABLE VII: The coefficients \bar{E}_k and \bar{F}_k of \bar{e}_r .

<i>Coefficient</i>	<i>Expression</i>
\bar{E}_4^{2PN}	$15(1111\eta^2 - 1624\eta + 528)$
\bar{E}_3^{2PN}	$4800(4\eta^2 - 7\eta + 4)$
\bar{E}_2^{2PN}	$-4(151\eta^2 - 7550\eta + 5640)$
\bar{E}_1^{2PN}	$2880(\eta - 3)\eta$
\bar{E}_0^{2PN}	$8(1501\eta^2 - 8090\eta + 7260)$
\bar{F}_8^{2PN}	$120(\eta - 3)\eta$
\bar{F}_7^{2PN}	$-60(44\eta^2 - 107\eta + 44)$
\bar{F}_6^{2PN}	$-15(317\eta^2 - 537\eta + 96)$
\bar{F}_5^{2PN}	$4(457\eta^2 - 1430\eta - 960)$
\bar{F}_4^{2PN}	$-5362\eta^2 + 18335\eta - 4380$
\bar{F}_3^{2PN}	$-6(714\eta^2 - 4315\eta + 5420)$
\bar{F}_2^{2PN}	$21(391\eta^2 - 2110\eta + 2100)$
\bar{F}_1^{2PN}	$-4(1411\eta^2 - 7820\eta + 7260)$
\bar{F}_0^{2PN}	$1501\eta^2 - 8090\eta + 7260$
\bar{E}^{SS}	$16e_{r0}^3(1 + e_{r0})^2\sqrt{1 - e_{r0}^2}(e_{r0}^2 + 2)$
\bar{F}^{SS}	$-[8(e_{r0} + 1)^2\sqrt{1 - e_{r0}^2} \times (e_{r0}^2 + 2)e_{r0}^3\cos(\zeta_1 - \zeta_2) + \cos(\zeta_1 + \zeta_2)[3176e_{r0}^3 - 3176e_{r0}^2 + 1552e_{r0}^4 - 1552e_{r0}^5 - 35e_{r0}^6 + \sqrt{1 - e_{r0}^2}(2376e_{r0}^2 - 2328e_{r0}^3 - 468e_{r0}^4 + 606e_{r0}^5 - 35e_{r0}^6 + 92e_{r0}^7 + 1600e_{r0} - 1600)]]$

TABLE VIII: The coefficients L_0 and K_0 .

<i>Coefficient</i>	<i>Expression</i>
$L_{0,2}^{2PN}$	$3(75\eta^2 - 176\eta + 216)$
$L_{0,1}^{2PN}$	$48(3\eta^2 - 11\eta + 10)$
$L_{0,0}^{2PN}$	$86\eta^2 - 260\eta + 176$
$K_{0,4}^{2PN}$	$12(12\eta^2 - 39\eta + 28)$
$K_{0,3}^{2PN}$	$-6(18\eta^2 - 63\eta + 64)$
$K_{0,2}^{2PN}$	$3(17\eta^2 - 7\eta + 28)$
$K_{0,1}^{2PN}$	$-2(7\eta^2 + 2\eta - 32)$
$K_{0,0}^{2PN}$	$43\eta^2 - 130\eta + 88$
L_0^{SS}	$4\bar{e}_r(4\bar{e}_r^4 + 53\bar{e}_r^3 + 78\bar{e}_r^2 + 72\bar{e}_r + 24)$
K_0^{SS}	$[-95\bar{e}_r^5 + 171\bar{e}_r^4 - 96\bar{e}_r^3 + 236\bar{e}_r^2 - 56\bar{e}_r + 32 - 32(1 - \bar{e}_r)(1 - \bar{e}_r^2)^{3/2}] \times \cos(\zeta_1 + \zeta_2) + 96\bar{e}_r^2 \times (1 + \bar{e}_r)^2(2\cos\zeta_1\cos\zeta_2 - \sin\zeta_1\sin\zeta_2) + 2\bar{e}_r(4\bar{e}_r^4 + 29\bar{e}_r^3 + 30\bar{e}_r^2 + 48\bar{e}_r + 24) \times \cos(\zeta_1 - \zeta_2)$

TABLE IX: The coefficients L_0 and K_0 .

<i>Coefficient</i>	<i>Expression</i>
$E_{0,4}^{2PN}$	$15 (2915\eta^2 - 8904\eta + 6192)$
$E_{0,3}^{2PN}$	$960 (36\eta^2 - 102\eta + 65)$
$E_{0,2}^{2PN}$	$4 (7673\eta^2 - 20110\eta + 15360)$
$E_{0,1}^{2PN}$	$960 (2\eta^2 - 11\eta + 15)$
$E_{0,0}^{2PN}$	$-8 (4559\eta^2 - 13390\eta + 9540)$
$F_{0,6}^{2PN}$	$15 (383\eta^2 - 989\eta + 560)$
$F_{0,5}^{2PN}$	$-30 (51\eta^2 - 261\eta + 224)$
$F_{0,4}^{2PN}$	$-15 (68\eta^2 - 301\eta + 232)$
$F_{0,3}^{2PN}$	$2 (893\eta^2 - 3505\eta + 3360)$
$F_{0,2}^{2PN}$	$-2 (1756\eta^2 - 6425\eta + 5250)$
$F_{0,1}^{2PN}$	$9358\eta^2 - 28100\eta + 20880$
$F_{0,0}^{2PN}$	$-4559\eta^2 + 13390\eta - 9540$
E_0^{SS}	$16\bar{e}_r^3 (1 + \bar{e}_r) (\bar{e}_r^3 + 3\bar{e}_r^2 + 4\bar{e}_r + 2)$
F_0^{SS}	$\cos(\zeta_1 + \zeta_2) [92\bar{e}_r^7 - 35\bar{e}_r^6$ $+ 606\bar{e}_r^5 - 468\bar{e}_r^4 - 2328\bar{e}_r^3$ $+ 2376\bar{e}_r^2 + 1600\bar{e}_r - 1600$ $+ 8(\bar{e}_r + 1)(3\bar{e}_r^2 + 200)(1 - \bar{e}_r)^{5/2}]$ $+ 32(\bar{e}_r + 1)^2\bar{e}_r^4$ $\times (2\cos\zeta_1\cos\zeta_2 - \sin\zeta_1\sin\zeta_2)$ $+ 8(\bar{e}_r + 1)^2(\bar{e}_r^2 + 2)\bar{e}_r^3$ $\times \cos(\zeta_1 - \zeta_2)$

-
- [1] J. Aasi et al. (LIGO Scientific), *Advanced LIGO*, Class. Quantum Grav., **32**, 074001, (2015).
- [2] B. P. Abbott et al. (LIGO Scientific, Virgo), *Observation of Gravitational Waves from a Binary Black Hole Merger*, Phys. Rev. Lett. **116**, 061102, (2016).
- [3] B. P. Abbott et al. (LIGO Scientific, Virgo), *GW151226: Observation of Gravitational Waves from a 22-Solar-Mass Binary Black Hole Coalescence*, Phys. Rev. Lett. **116**, 241103, (2016).
- [4] K. Chatziioannou, A. Klein, N. Cornish, N. Yunes, *Analytic gravitational waveforms for generic precessing compact binaries*, arXiv:1606.03117 [gr-qc] (2016).
- [5] A. Klein, N. Cornish, N. Yunes, *Fast Frequency-domain Waveforms for Spin-Precessing Binary Inspirals*, Phys. Rev. D **90**, 124029 (2014).
- [6] N. J. Cornish, J. S. Key, *Computing waveforms for spinning compact binaries in quasi-eccentric orbits*, Phys. Rev. D **82**, 044028 (2011).
- [7] B. Mikóczi, P. Forgács, M. Vasúth, *Eccentric first post-Newtonian waveforms for compact binaries in frequency domain with Hansen coefficients*, Phys. Rev. D **92**, 044038 (2015).
- [8] P. Schmidt, F. Ohme, M. Hannam, *Towards models of gravitational waveforms from generic binaries II: Modelling precession effects with a single effective precession parameter*, Phys. Rev. D **91**, 024043 (2015).
- [9] Y. Pan, A. Buonanno, A. Taracchini, L. E. Kidder, A. H. Mroue, H. P. Pfeiffer, M. A. Scheel, B. Szilagyi, *Inspiral-merger-ringdown waveforms of spinning, precessing black-hole binaries in the effective-one-body formalism*, Phys. Rev. D **89**, 084006 (2014).
- [10] M. Hannam, P. Schmidt, A. Bohé, L. Haegel, S. Husa, F. Ohme, G. Pratten, M. Pürrer, *A simple model of complete precessing black-hole-binary gravitational waveforms*, Phys. Rev. Lett. **113**, 151101 (2014).
- [11] A. Gupta, A. Gopakumar, *Post-newtonian analysis of precession convention for spinning compact binaries*, Class. Quantum Grav. **32**, 175002, (2015).
- [12] D. Bini, F. de Felice, A. Gericco, R. T. Jantzen, *Spin precession along circular orbits in the Kerr spacetime: the Frenet-Serret description*, Class. Quantum Grav. **23**, 3287 (2006).
- [13] B. Farr, E. Ochsner, W. M. Farr, R. O'Shaughnessy, *A more effective coordinate system for parameter estimation of precessing compact binaries from gravitational waves*, Phys. Rev. D **90**, 024018 (2014).
- [14] S. R. Dolan, N. Warburton, A. I. Harte, A. Le Tiec, B. Wardell, L. Barack, *Gravitational self-torque and spin precession in compact binaries*, Phys. Rev. D **89**, 064011 (2014).
- [15] D. Bini, T. Damour, *Analytic determination of high-order post-Newtonian self-force contributions to gravitational spin precession*, Phys. Rev. D **91**, 064064 (2015).
- [16] B. Mikóczi, *Spin supplementary conditions for spinning compact binaries*, [arXiv:1609.01536] (2016).
- [17] R. Rieth and G. Schäfer, *Spin and tail effects in the gravitational-wave emission of compact binaries*, Class. Quantum Grav. **14**, 2357 (1997).
- [18] E. Poisson, *Gravitational waves from inspiraling compact binaries: The quadrupole-moment term*, Phys. Rev. D **57**, 5287 (1998).
- [19] L. Á. Gergely, Z. I. Perjés, M. Vasúth, *Spin effects in gravitational radiation backreaction III. Compact binaries with two spinning components*, Phys. Rev. D **58**, 124001 (1998). [arXiv:gr-qc/9808063]
- [20] L. Á. Gergely, *Spin-spin effects in radiating compact binaries*, Phys. Rev. D **61** 024035 (2000).
- [21] L. Á. Gergely, Z. Keresztes, *Gravitational radiation reaction in compact binary systems: Contribution of the quadrupole-monopole interaction*, Phys. Rev. D **67** 024020 (2003).
- [22] C. M. Will, *Post-Newtonian gravitational radiation and equations of motion via direct integration of the relaxed Einstein equations. III. Radiation reaction for binary systems with spinning bodies*, Phys. Rev. D **71**, 084027 (2005).
- [23] B. Mikóczi, M. Vasúth, L. Á. Gergely, *Self-interaction spin effects in inspiraling compact binaries*, Phys. Rev. D **71**, 124043 (2005).
- [24] J. Zeng, C. M. Will, *Application of energy and angular momentum balance to gravitational radiation reaction for binary systems with spin-orbit coupling*, Gen Relativ Gravit **39** 1661 (2007).
- [25] H. Wang, C. M. Will, *Post-Newtonian gravitational radiation and equations of motion via direct integration of the relaxed Einstein equations. IV. Radiation reaction for binary systems with spin-spin coupling*, Phys. Rev. D **75**, 064017 (2007).
- [26] J. Majár, M. Vasúth, *Gravitational waveforms for spinning compact binaries*, Phys. Rev. D **77**, 104005 (2008).
- [27] Th. Damour, P. Jaranowski, and G. Schäfer, *Hamiltonian of two spinning compact bodies with next-to-leading order gravitational spin-orbit coupling*, Phys. Rev. D **77**, 064032 (2008).
- [28] J. Steinhoff, G. Schäfer, and S. Hergt, *ADM canonical formalism for gravitating spinning objects*, Phys. Rev. D **77**, 104018 (2008).
- [29] Th. Damour, P. Jaranowski, and G. Schäfer, *Effective one body approach to the dynamics of two spinning black holes with next-to-leading order spin-orbit coupling*, Phys. Rev. D **78**, 024009 (2008).
- [30] E. E. Flanagan and T. Hinderer, *Evolution of the Carter constant for inspirals into a black hole: Effect of the black hole quadrupole*, Phys. Rev. D **75**, 124007 (2007).
- [31] É. Racine, *Analysis of spin precession in binary black hole systems including quadrupole-monopole interaction*, Phys. Rev. D **78**, 044021 (2008).
- [32] E. Barausse, É. Racine, and A. Buonanno, *Hamiltonian of a spinning test particle in curved spacetime*, Phys. Rev. D **80**, 104025 (2009).
- [33] J. Majár, *Spin-spin interaction in the spin-precession equations*, Phys. Rev. D **80**, 104028 (2009).
- [34] K. G. Arun, A. Buonanno, G. Faye, and E. Ochsner, *Higher-order spin effects in the amplitude and phase of gravitational waveforms emitted by inspiraling compact binaries: Ready-to-use gravitational waveforms*, Phys. Rev. D **79**, 104023 (2009).
- [35] A. Klein, P. Jetzer, *Spin effects in the phasing of gravitational waves from binaries on eccentric orbits*, Phys. Rev. D **81**, 124001 (2010).
- [36] J. Steinhoff and H. Wang, *Canonical formulation of grav-*

- itating spinning objects at 3.5 post-Newtonian order, Phys. Rev. D **81**, 024022 (2010).
- [37] X. Wu and Y. Xie, *Symplectic structure of post-Newtonian Hamiltonian for spinning compact binaries*, Phys. Rev. D **81**, 084045 (2010).
- [38] G. Faye, L. Blanchet, B. R. Iyer, *Non-linear multipole interactions and gravitational-wave octupole modes for inspiralling compact binaries to third-and-a-half post-Newtonian order*, Class. Quantum Grav. **32**, 045016 (2015).
- [39] A. Bohé, G. Faye, S. Marsat, E. K Porter, *Quadratic-in-spin effects in the orbital dynamics and gravitational-wave energy flux of compact binaries at the 3PN order*, Class. Quantum Grav. **32**, 19 (2015).
- [40] S. Ossokine, M. Boyle, L. E. Kidder, H. P. Pfeiffer, M. A. Scheel, B. Szilágyi, *Comparing Post-Newtonian and Numerical-Relativity Precession Dynamics*, Phys. Rev. D **92**, 104028 (2015).
- [41] I. Harry, S. Privitera, A. Bohé, A. Buonanno, *Searching for Gravitational Waves from Compact Binaries with Precessing Spins*, arXiv:1603.02444 [gr-qc] (2016).
- [42] T. Dal Canton, A. P. Lundgren, A. B. Nielsen, *Impact of precession on aligned-spin searches for neutron-star-black-hole binaries*, Phys. Rev. D **91**, 062010 (2015).
- [43] R. O'Shaughnessy, B. Farr, E. Ochsner, H.S. Cho, V. Raymond, C. Kim, C.H. Lee, *Parameter Estimation of Gravitational Waves from Precessing BH-NS Inspirals with higher harmonics*, Phys. Rev. D **89**, 102005 (2014).
- [44] M. Levi, J. Steinhoff, *Complete conservative dynamics for inspiralling compact binaries with spins at fourth post-Newtonian order*, arXiv:1607.04252 [gr-qc]
- [45] B. P. Abbott et al. (LIGO Scientific, Virgo), *An improved analysis of GW150914 using a fully spin-precessing waveform model*, arXiv:1606.01210 [gr-qc]
- [46] L. Á. Gergely, P. L. Biermann, *The spin-flip phenomenon in supermassive black hole binary mergers*, Astrophys. J. **697**, 1621, (2009).
- [47] Gopal-Krishna, P.L. Biermann, L.Á. Gergely, P.J. Wiita, *On the origin of X-shaped radio galaxies*, Res. Astron. Astrophys. **12**, 127 (2012).
- [48] T. A. Apostolatos, C. Cutler, G. J. Sussman, K. S. Thorne, *Spin-induced orbital precession and its modulation of the gravitational waveforms from merging binaries*, Phys. Rev. D **49**, 6274 (1994).
- [49] E. Kun, K. É. Gabányi, M. Karouzos, S. Britzen, L. Á. Gergely, *A spinning supermassive black hole binary model consistent with VLBI observations of the S5 1928+738 jet*, Mon. Not. Royal Astron. Soc. **445** (2), 1370 (2014).
- [50] L. Á. Gergely, *Spinning compact binary inspiral: Independent variables and dynamically preserved spin configurations*, Phys. Rev. D **81**, 084025 (2010).
- [51] L. Á. Gergely, *Spinning compact binary inspiral. II. Conservative angular dynamics*, Phys. Rev. D **82**, 104031 (2010). E-print: arXiv:1005.5330.
- [52] L. Á. Gergely, Z. Keresztes, *Spinning compact binary dynamics and chameleon orbits*, Phys. Rev. D **91**, 024012 (2015). [arXiv:1411.4057 [gr-qc]]
- [53] T. Damour, N. Deruelle, *General relativistic celestial mechanics of binary systems. I. The post-Newtonian motion*, Ann. Inst. Henri Poincaré (Phys. Théor.) **43**, 107 (1985).
- [54] L. Blanchet, *Gravitational Radiation from Post-Newtonian Sources and Inspiralling Compact Binaries*, Living Rev. Relativity **17**, 2 (2014).
- [55] B. M. Barker, R. F. O'Connell, *Gravitational two-body problem with arbitrary masses, spins, and quadrupole moments*, Phys. Rev. D **12**, 329 (1975); Gen. Relativ. Gravit. **2**, 1428 (1979).
- [56] L. E. Kidder, C.M. Will, A. G. Wiseman, *Spin effects in the inspiral of coalescing compact binaries*, Phys. Rev. D **47**, R4183 (1993).
- [57] L. E. Kidder, *Coalescing binary systems of compact objects to (post)^{5/2}-Newtonian order. V. Spin effects*, Phys. Rev. D **52**, 821 (1995).
- [58] Z. Keresztes, B. Mikóczi, L. Á. Gergely, *Kepler equation for inspiralling compact binaries*, Phys. Rev. D **72**, 104022 (2005).
- [59] C. O. Lousto, J. Healy, *Flip-flopping binary black holes*, Phys. Rev. Lett. **114**, 141101 (2015). [arXiv:1410.3830]
- [60] C. O. Lousto, J. Healy, *Unstable flip-flopping spinning binary black holes*, Phys. Rev. D **93**, 124074 (2016).
- [61] C. O. Lousto, J. Healy, H. Nakano, *Spin flips in generic black hole binaries*, Phys. Rev. D **93**, 044031 (2016). [arXiv:1506.04768]